Trends In Carbohydrate Research, Vol.15, No.1 (2023) 62-90 0975-0304/09

Trends in Carbohydrate Research

Glucopyranoside Derivatives as Potential Antimicrobial Agents: Synthesis, Anticancer, DFT, Molecular Docking, Molecular Dynamics and ADMET Predictions

Sajia Islam,[1] Shopnil Akash,[2] Jannatul Ferdous,[1] Ajoy Kumer,[3] Mohammed Al-Ghorbani,[4] Mohammed Baashen,[5] Abdullah M. Shbeer,[6] Mohammed Ageel,[7] Unesco Chakma,[8] Imtiaj Hasan,[9] Sultana Rajia,[10] Yuki Fujii,[11] Yasuhiro Ozeki,[12] and Sarkar M. A. Kawsar[1,*]

[1]*Department of Chemistry, Lab of Carbohydrate and Nucleoside Chemistry (LCNC), Faculty of Science, University of Chittagong, Chittagong-4331, Bangladesh*

[2]*Department of Pharmacy, Daffodil International University, Sukrabad, Dhaka-1207, Bangladesh*

[3]*Department of Chemistry, European University of Bangladesh, Gabtoli, Dhaka-1216, Bangladesh*

[4]*Department of Chemistry, Faculty of Science and Arts, Ulla, Taibah University, Medina 41477, Saudi Arabia*

[5]*Department of Chemistry, Science and Humanities College, Shaqra University, Saudi Arabia*

[6]*Department of Surgery, Faculty of Medicine, Jazan University, Jazan 45142, Saudi Arabia*

[7]*Department of Surgery, Faculty of Medicine, Jazan University, Jazan 45142, Saudi Arabia*

[8]*Department of Electrical and Electronics Engineering, European University of Bangladesh, Gabtoli, Dhaka-1216, Bangladesh*

[9]*Department of Biochemistry and Molecular Biology, Faculty of Science, University of Rajshahi, Rajshahi-6205, Bangladesh*

[10]*Center for Interdisciplinary Research, Varendra University, Rajshahi-6204, Bangladesh0*

[11]*Department of Pharmacy, Faculty of Pharmaceutical Science, Nagasaki International University, 2825-7 Huis Ten Bosch, Sasebo, Nagasaki 859-3298, Japan*

[12]*School of Sciences, Yokohama City University, 22-2, Seto, Kanazawa-ku, Yokohama 236-0027, Japan*

This paper has been dedicated to Professor Bishnu P. Chatterjee on his 80th birthday.

Received October 29, 2022; Accepted March 27, 2023

Graphical Abstract

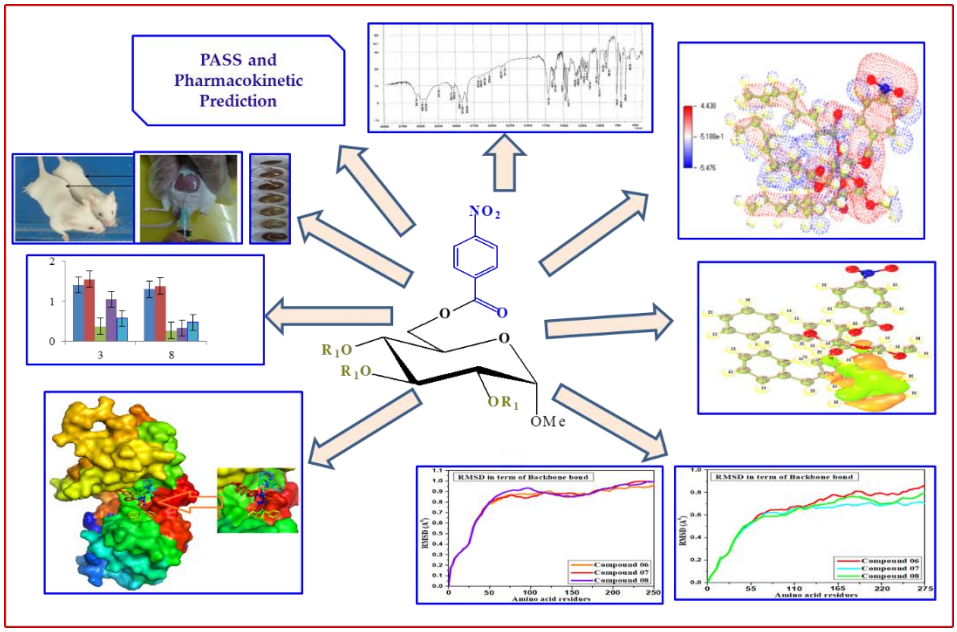

* Corresponding author: Sarkar M. A. Kawsar
e-mail: akawsarabe@yahoo.com
Tel.: +88-01762717081

Abstract

Methyl α-D-glucopyranoside and its seven acylated derivatives have been used to develop antibacterial and antifungal drugs by using in silico and *in vitro* antimicrobial functionality tests against five pathogenic bacteria and two fungi. Methyl α-D-glucopyranoside derivatives (**1-8**) were synthesized, purified, and characterized by physicochemical, elemental, and spectroscopic methods. Compounds **3** (zone of inhibition, 22±0.3 mm) and **8** (zone of inhibition, 24±0.4 mm) showed the highest inhibition against *Bacillus subtilis* and *Staphylococcus aureus*. A MIC value of 0.275±0.01 mg/ml was found for derivative **8** against *S. ebony* whereas the MBC value recorded for derivative **3** against *S. aureus* was 1.70±0.01 mg/ml. Most of these derivatives showed >78% inhibition of fungal mycelial growth. The *in vitro* effect of compound **8** against Ehrlich ascites carcinoma (EAC) cells, by MTT colorimetric assay, showed 25.97% of cell growth inhibition with an IC_{50} value of 1024.83 µg/ml. A DFT technique was used to determine the Highest Occupied Molecular Orbital (HOMO) and Lowest Unoccupied Molecular Orbital (LUMO), and the energy gap between them. Furthermore, the chemical reactivity and global descriptors were computed from the HOMO and LUMO values. The most crucial aspect of this research is the molecular docking against two gram-positive bacterial proteins (*B. subtilis* and *S. aureus)*, two gram-negative bacterial proteins (*Escherichia coli* and *Pseudomonas aeruginosa*), and six fungal proteins (*Aspergillus niger*, *Aspergillus flavus*, *Rhizomucor miehei*, *Mucor lusitanicus*, *Candida albicans* and *Candida Auris*). In most cases, docking scores crossed the scores of the standard drugs, Azithromycin and Nystatin. A 100-ns molecular dynamics (MD) simulation study revealed stable conformation and binding patterns/energy in a stimulating environment. The range of quantitative structure-activity relationship (QSAR) and pIC_{50} found was between 4.19–9.15, signifying these compounds to be physiologically effective towards microbes. Most importantly, these compounds are non–carcinogenic, have low toxicity in aquatic and non–aquatic species, and are highly soluble in water and stable, indicating the suitability of these compounds as antimicrobial agents for therapeutic and drug development purposes.

Keywords: Synthesis; Glucopyranoside; Docking; Molecular dynamics and Antifungal/anticancer

1. Introduction

The most prevalent biochemical components and materials in living cells are carbon-containing (organic) molecules and water (70% of the cell's volume),[1] which are required for a significant portion of the metabolism of all living beings.[2] Carbohydrates are also been referred to as glucose,[3] sucrose, saccharides, and glycans,[4] and they are the most significant and frequently distributed macromolecules in nature.[5] In any organism, carbohydrates are frequently associated with proteins and lipids, as well as other metabolites, and are termed glycoconjugates.[6] The fundamental function of carbohydrates is in a wide range of physiological activities that serve as the body's key functions.[7] They carry genetic information processed by carbohydrate-binding proteins (such as lectins).[8] As a new approach, these functional carbohydrates can lead us to novel drug discovery[9] through the development of targeted therapies like cancer vaccines, HIV/AIDS Vaccines,[10] Diabetes and Alzheimer's disease[11] Nano Pills, antiviral drugs[12] and antibacterial.[13-16]

Bacteria are known as prokaryotic single-celled germs with no nuclear envelope that seem to be metabolically active and proliferate through binary fission.[17] These microorganisms can be differentiated by the structure of their cell walls, sizes, or variations in genetic composition.[18] However, there are different classes of antibiotics available on the market to fight against pathogenic bacteria,[19] such as penicillin, azithromycin, and ciprofloxacin. However, in the present era of modern healthcare, a significant number of patients have perished as a result of antibacterial resistance.[20] It has been seen that, already, a variety of antibiotics have lost their efficacy against different bacteria, which includes penicillin-resistant *Staphylococcus aureus*,[21] Ciprofloxacin-resistant *Neisseria gonorrhoeae*,[22] *and* Azithromycin-resistant *Neisseria gonorrhoeae*.[23]

During the last few years, fungal infections increased at an alarming rate, creating prominent health concerns. Moreover, a quarter of (20–25% or 1.7 billion people) the world's population has been infected by fungi on their skin or nails. Researchers have identified about 1.5 million fungal species, and of those, more than 8,000 have been reported as pathogens in plants, with another 300 shown to be harmful to humans.[24] The most prevalent fungal pathogens in mammals comprise Candida, Aspergillus, Pneumocystis, and Cryptococcus spp. fungal infections are thought to have triggered 25–73.7% of all SARS-related fatalities during the Covid-19 Pandemic.[25] Fungicide drugs like azoles and fluconazole have been used worldwide to combat fungal infections. However, research has revealed fluconazole-resistant *Candida albicans*,[26] amphotericin B, and fluconazole-resistant *Candida auris*;[27] particularly notable is *Candida* and *Aspergillus* infestations, whose treatment options are constrained. One of the most significant impacts on human health concerns now is the development of multidrug-resistant *Candida glabrata* and *Candida auris.*[28] Therefore, to combat these fatal pathogens, an antifungal medication that is both effective and efficient is desperately required. Glucopyranoside is one of the most significant and potent classes of carbohydrates due to the numerous biological applications of its analogs.[29-33]

Since glucopyranoside and its analogs have demonstrated multiple bioactivities, this supports the

synthesis and investigation of an effective antibacterial and antifungal drug. Therefore, the carbohydrate-containing compound glucopyranoside and its derivatives have been selected, and different assays were performed against different bacteria and pathogenic fungi, including black and white fungi. A variety of complexity and risks are associated with the design and development of a new medication process. Developing a new medicine has already become very costly and takes 10 to 15 years. That is why new computational approaches are necessary for this purpose.

2. Experimental

2.1. Materials

All reagents used are commercially available (Sigma-Aldrich). Melting points (m.p.) were determined using an electrothermal m.p. apparatus (England). Evaporations were performed under reduced pressure on a Buchi rotary evaporator (MilliporeSigma; Germany). Infrared spectral analyses were performed using a Fourier-transform infrared (FTIR) spectrophotometer (IR Prestige-21, Shimadzu, Japan). ^{1}H-NMR spectra in $CDCl_3$ (δ in ppm) were recorded with tetramethylsilane as the internal standard. Column chromatography was performed using silica gel G_{60}. $CHCl_3$/CH_3OH mixture in various proportions was used as a solvent system for TLC analyses.

2.2. Synthesis

A solution of methyl α-D-glucopyranoside (**1**) (100 mg, 1.04 mmol) in anhydrous *N*,*N*-dimethylformamide (DMF) (~3 ml), and triethylamine (6-7 drops) was prepared, cooled to 0°C, treated with 1.1 molar eq. of 4-nitrobenzoyl chloride (90.0 mg) with continuous stirring at 0°C for 6 h, and stirring continued at room temperature. The progress of the reaction was monitored by TLC (CH_3OH/ $CHCl_3$, 1:4) to confirm the full conversion of the starting material to a single product. Ice was added to the flask to eliminate excess reagent, and the contents were extracted using chloroform (3×10 ml). The combined $CHCl_3$ layer was washed successively with dilute HCl (10%), saturated aqueous (sat. aq.) $NaHCO_3$ solution, and distilled water. The organic layer was dried with $MgSO_4$, filtered, and the filtrate concentrated under reduced pressure. The resulting syrupy mass was subjected to silica gel column chromatographic purification (with CH_3OH/ $CHCl_3$, 1/4 as eluent; R_f = 0.52) to yield the title compound (**2**) (253 mg).

2.2.1. Methyl 6-*O*-(4-nitrobenzoyl)-α-D-glucopyranoside (**2**). White, amorphous solid, yield 84.58%, Mp 78–80 °C, IR (KBr) ν/cm^{-1} 1701 (C=O), 3410-3510 (-OH); ^{1}H-NMR (400 MHz, $CDCl_3$) δ_H 8.28 (2H, d, Ar-H), 8.21 (2H, d, Ar-H), 4.98 (1H, d, H-1), 4.97 (1H, dd, H-6a), 4.95 (1H, dd, H-6b), 4.27 (1H, t, H-4), 3.99 (1H, t, H-3), 3.77 (1H, dd, H-2), 3.65 (1H, ddd, H-5), 3.41 (3H, s, 1-OCH_3); ^{13}C-NMR (100 MHz, $CDCl_3$): δ_C 178.12 (4-NO_2.C_6H_4.*C*O-), 150.86, 134.18, 130.90, 130.83, 123.64, 123.61 (4-NO_2.*C*$_6H_4$CO-), 106.10 (C-1), 78.91 (C-2), 77.09 (C-4), 76.61 (C-3), 69.15 (C-5), 62.05 (C-6), 59.06 (1-O*C*H_3); LC-MS $[M+1]^+$ 344.29. Analysis calcd for $C_{14}H_{17}O_7NO_2$: C, 48.97, H, 4.99%; found: C, 48.99, H, 5.01%.

2.2.2. General procedure for the synthesis of (4-nitrobenzoyl)-α-D-glucopyranoside derivatives (3-8)

Octanoyl chloride (0.838 ml, 5 molar eq.) was added to a cooled (-5°C), stirred solution of triol **2** (297 mg, 0.90 mmol) in dry DMF (3 ml) with triethylamine (6-7 drops)., and stirring continued at -5°C for 6-7 h. The progress of the reaction was monitored by TLC (CH_3OH/ $CHCl_3$, 1:4) to confirm the complete conversion of the reactant to a single product (R_f = 0.51). The syrupy residue was passed through a silica gel column and eluted with CH_3OH/$CHCl_3$ (1:4) to yield octanoyl derivative (**3**) (254.1 mg) as a crystalline solid.

Similar reactions of compounds **4**, **5**, **6**, **7**, and **8** yielded, respectively, palmitoyl derivative (221.3 mg), stearoyl derivative (734 mg), trityl derivative (176.6 mg), cinnamoyl derivative (145 mg), and 4-t-butylbenzoyl derivative (621 mg).

2.2.3. Methyl 6-*O*-(4-nitrobenzoyl)-2,3,4-tri-*O*-octanoyl-α-D-glucopyranoside (**3**). White, crystalline solid, yield 85.28%, Mp 105–106 °C, IR (KBr) ν/cm^{-1} 1705 (C=O); ^{1}H-NMR (400 MHz, $CDCl_3$) δ_H 8.28 (2H, d, Ar-H), 8.22 (2H, d, Ar-H), 5.45 (1H, d, H-1), 5.22 (1H, m, H-2), 5.06 (1H, t, H-3), 4.88 (1H, m, H-4), 4.18 (1H, dd, H-6a), 4.11 (1H, m, H-6b), 3.97 (1H, m, H-5), 3.36 (3H, s, 1-OCH_3), 2.37 {6H, m, 3×$CH_3(CH_2)_5CH_2CO$-}, 1.59 {6H, m, 3×$CH_3(CH_2)_4CH_2CH_2CO$-}, 1.28 {24H, m, 3×$CH_3(CH_2)_4(CH_2)_2CO$-}, 0..88 {9H, m, 3×$CH_3(CH_2)_6CO$-}; ^{13}C-NMR (100 MHz, $CDCl_3$): δ_C 178.0 (4-NO_2.C_6H_4.*C*O-), 171.0, 170.75, 170.11 {3×$CH_3(CH_2)_6$*C*O-}, 150.74, 134.11, 130.76, 130.45, 123.09, 123.01 (4-NO_2.*C*$_6H_4$CO-), 105.34 (C-1), 78.76 (C-2), 76.11 (C-4), 75.89 (C-3), 69.12 (C-5), 62.21 (C-6), 59.45 (1-O*C*H_3), 34.21, 34.11 (×3), 34.07, 32.0 (×2), 29.11 (×2), 25.13 (×3), 22.61, 22.02, 20.17 (×3), 20.02 {3×CH_3(*C*H_2)$_6$CO-}, 14.01, 13.88, 13.52 {3×*C*$H_3(CH_2)_6CO$-}; LC-MS $[M+1]^+$ 722.87. Analysis calcd for $C_{38}H_{59}O_{10}NO_2$: C, 63.23, H, 8.23%; found: C, 63.25, H, 8.22%.

2.2.4. Methyl 6-*O*-(4-nitrobenzoyl)-2,3,4-tri-*O*-palmitoyl-α-D-glucopyranoside (**4**). White, as needles, yield 90.10%, Mp 110–111 °C, IR (KBr) ν/cm^{-1} 1731 (C=O); ^{1}H-NMR (400 MHz, $CDCl_3$) δ_H

8.28 (2H, d, Ar-H), 8.20 (2H, d, Ar-H), 5.21 (1H, d, H-1), 4.97 (1H, dd, H-2), 4.69 (1H, t, H-3), 4.64 (1H, t, H-4), 3.96 (1H, dd, H-6b), 3.85 (1H, dd, H-6a), 3.82 (1H, m, H-5), 3.43 (3H, s, 1-OCH_3), 2.34 {6H, m, 3×$CH_3(CH_2)_{13}CH_2CO$-}, 1.63 {6H, m, 3×$CH_3(CH_2)_{12}CH_2CH_2CO$-}, 1.29 {72H, m, 3×$CH_3(CH_2)_{12}CH_2CH_2CO$-}, 0.88 {9H, m, 3×$CH_3(CH_2)_{14}CO$-}; ^{13}C-NMR (100 MHz, $CDCl_3$): δ_C 177.92 (4-NO_2.C_6H_4.*C*O-), 172.21, 172.11, 171.91 {3×$CH_3(CH_2)_{14}$*C*O-}, 151.02, 134.23, 130.45, 130.11, 124.03, 123.81 (4-NO_2.*C*$_6H_4$CO-), 105.78 (C-1), 77.96 (C-2), 77.12 (C-4), 76.53 (C-3), 69.11 (C-5), 62.55 (C-6), 59.02 (1-O*C*H_3), 34.43, 34.38, 34.36, 34.12 (×2), 31.95, 31.91(×2), 31.87 (×3), 29.52 (×2), 29.15, 29.31, 29.26 (×3), 29.13 (×3), 29.11, 25.11 (×2), 24.77, 24.63, 22.61 (×3), 22.60, 22.55 (×3), 22.31 (×2), 21.65(×2), 21.54, 20.04 (×3), 20.01 {3×CH_3(*C*H_2)$_{14}$CO-}, 14.11, 14.08, 14.02 {3×*C*H_3(CH_2)$_{12}$CO-}; LC-MS $[M+1]^+$ 1059.51. Analysis calcd for $C_{62}H_{107}O_{10}NO_2$: C, 70.35, H, 10.18%; found: C, 70.36, H, 10.19%.

2.2.5. Methyl 6-*O*-(4-nitrobenzoyl)-2,3,4-tri-*O*-stearoyl-α-D-glucopyranoside (**5**). White, crystalline solid, yield 89.73%, Mp 116–117 °C, IR (KBr) ν/cm^{-1} 1682 (C=O); ^{1}H-NMR (400 MHz, $CDCl_3$) δ_H 8.29 (2H, d, Ar-H), 8.18 (2H, d, Ar-H), 5.18 (1H, d, H-1), 4.99 (1H, dd, H-2), 4.87 (1H, t, H-3), 4.75 (1H, t, H-4), 3.99 (1H, dd, H-6b), 3.87 (1H, dd, H-6a), 3.81 (1H, m, H-5), 3.41 (3H, s, 1-OCH_3), 2.38 {4H, m, 2×$CH_3(CH_2)_{15}CH_2CO$-}, 1.26 {60H, m, 2×$CH_3(CH_2)_{15}CH_2CO$-}, 0.99 {6H, m, 2×$CH_3(CH_2)_{16}CO$-}; ^{13}C-NMR (100 MHz, $CDCl_3$): δ_C 178.09 (4-NO_2.C_6H_4.CO-), 172.21, 172.11, 171.91 {3×$CH_3(CH_2)_{16}$*C*O-}, 150.92, 134.10, 130.55, 130.96, 123.44, 123.61 (4-NO_2.*C*$_6H_4$CO-), 106.11 (C-1), 78.96 (C-2), 78.64 (C-4), 76.69 (C-3), 69.53 (C-5), 62.83 (C-6), 59.82 (1-O*C*H_3); 34.43, 34.38, 34.36, 34.12 (×3), 31.95, 31.91(×3), 31.87 (×4), 29.52 (×3), 29.15, 29.31, 29.26 (×3), 29.13 (×3), 29.11, 25.11 (×2), 24.77, 24.63, 22.61 (×3), 22.60, 22.55 (×3), 22.31 (×3), 21.65(×2), 21.54, 20.04 (×4), 20.01 {3×CH_3(*C*H_2)$_{16}$CO-}, 14.11, 14.08, 14.02 {3×*C*H_3(CH_2)$_{16}$CO-}; LC-MS $[M+1]^+$ 1143.67. Analysis calcd for $C_{68}H_{119}O_{10}NO_2$: C, 71.48, H, 10.49%; found: C, 71.46, H, 10.51%.

2.2.6. Methyl 6-*O*-(4-nitrobenzoyl)-2,3,4-tri-*O*-trityl-α-D-glucopyranoside (**6**). White, crystalline solid, yield 99.58%, Mp 150–151 °C, IR (KBr) ν/cm^{-1} 1738 (C=O); ^{1}H-NMR (400 MHz, $CDCl_3$) δ_H 8.31 (2H, d, Ar-H), 8.17 (2H, d, Ar-H), 7.56 (18H, m, 3×Ar-H), 7.34 (27H, m, 3×Ar-H), 5.22 (1H, d, H-1), 5.06 (1H, dd, H-2), 4.89 (1H, t, H-3), 4.77 (1H, t, H-4), 4.09 (1H, dd, H-6b), 3.89 (1H, dd, H-6a), 3.85 (1H, m, H-5), 3.43 (3H, s, 1-OCH_3); ^{13}C-NMR (100 MHz, $CDCl_3$): δ_C 178.11 (4-NO_2.C_6H_4.*C*O-), 150.22, 135.02, 130.93, 130.45, 124.11, 123.75 (4-NO_2.*C*$_6H_4$CO-), 146.09 (×3, C-1), 145.68 (×3, C-1), 145.20 (×3, C-1), 129.54 (×6, C-2), 129.51 (×6, C-2), 129.42 (×6, C-2), 127.84 (×3, C-3), 127.84 (×3, C-3), 127.84 (×3, C-3), 127.77 (×6, C-4), 127.68 (×6, C-4), 127.53 (×6, C-4) {3×(*C*$_6H_5$)$_3$C-}, 106.16 (C-1), 78.35 (C-2), 77.11 (C-4), 76.10 (C-3), 69.01 (C-5), 62.43 (C-6), 59.11 (1-O*C*H_3), 81.86 (×3, C-5), 81.42 (×3, C-5), 81.28 (×3, C-5) {3×(C_6H_5)$_3$*C*-}; LC-MS $[M+1]^+$ 1071.23. Analysis calcd for $C_{71}H_{59}O_7NO_2$: C, 79.68, H, 5.55%; found: C, 79.67, H, 5.57%.

2.2.7. Methyl 2,3,4-tri-*O*-cinnamoyl-6-*O*-(4-nitrobenzoyl)-α-D-glucopyranoside (**7**). White, crystalline solid, yield 95.0%, Mp 122–123 °C, IR (KBr) ν/cm^{-1} 1716 (C=O), 1630 (-CH=CH-); ^{1}H-NMR (400 MHz, $CDCl_3$) δ_H 8.29 (2H, d, Ar-H), 7.80 (2H, d, Ar-H), 7.76 (6H, m, Ar-H), 7.55, 7.50, 7.40 (3×1H, 3×d, 3×PhCH=CHCO-), 7.28 (9H, m, Ar-H), 6.48, 6.41, 6.38 (3×1H, 3×d, 3×PhCH=CHCO-), 4.88 (1H, d, H-1), 4.76 (1H, dd, H-2), 4.73 (1H, t, H-3), 4.70 (1H, t, H-4), 4.00 (1H, dd, H-6b), 3.88 (1H, dd, H-6a), 3.73 (1H, m, H-5), 3.23 (3H, s, 1-OCH_3); ^{13}C-NMR (100 MHz, $CDCl_3$): δ_C 177.88 (4-NO_2.C_6H_4.*C*O-), 165.84, 165.78, 165.55 (3×C_6H_5CH=CH*C*O-), 151.11, 135.10, 131.14, 130.56, 124.04, 123.55 (4-NO_2.*C*$_6H_4$CO-), 150.57, 150.35, 149.97 (3×C_6H_5*C*H=CHCO-), 132.99, 132.81 (×4), 132.76, 132.21, 129.20 (×5), 129.12, 129.08 (×4), 129.01 (3×*C*$_6H_5$CH=CHCO-), 122.06, 121.88, 121.32 (3×C_6H_5CH=*C*HCO-), 106.21 (C-1), 78.28 (C-2), 77.25 (C-4), 76.81 (C-3), 69.10 (C-5), 62.11 (C-6), 59.15 (1-O*C*H_3); LC-MS $[M+1]^+$ 734.72. Analysis calcd for $C_{41}H_{35}O_{10}NO_2$: C, 67.12, H, 4.80%; found: C, 67.13, H, 4.82%.

2.2.8. Methyl 2,3,4-tri-*O*-(4-*t*-butylbenzoyl)-6-*O*-(4-nitrobenzoyl)-α-D-glucopyranoside (**8**). White, needles, yield 97.0%, Mp 140–141 °C, IR (KBr) ν/cm^{-1} 1722 (C=O); ^{1}H-NMR (400 MHz, $CDCl_3$) δ_H 8.30 (2H, d, Ar-H), 8.06 (2H, d, Ar-H), 7.51 (6H, m, 3×Ar-H), 7.28 (6H, m, 3×Ar-H), 4.91 (1H, d, H-1), 4.87 (1H, dd, H-2), 4.84 (1H, t, H-3), 4.81 (1H, t, H-4), 4.08 (1H, dd, H-6b), 4.00 (1H, dd, H-6a), 3.25 (1H, m, H-5), 3.03 (3H, s, 1-OCH_3), 1.32, 1.28, 1.24{27H, 3×s, 3×$(CH_3)_3$C-}; ^{13}C-NMR (100 MHz, $CDCl_3$): δ_C 178.0 (4-NO_2.C_6H_4.*C*O-), 174.40, 174.23, 174.11 {3×$(CH_3)_3CC_6H_4$*C*O-}, 150.15, 134.56, 131.84, 130.23, 124.33, 123.34 (4-NO_2.*C*$_6H_4$CO-), 132.44 (×3), 132.40 (×2), 132.40, 130.94 (×3), 129.91 (×3), 126.52 (×3), 125.50 (×3) {3×$(CH_3)_3$C*C*$_6H_4$CO-}, 107.11 (C-1), 79.45 (C-2), 78.0 (C-4), 76.44 (C-3), 69.10 (C-5), 62.09 (C-6), 59.01 (1-O*C*H_3), 35.60, 35.57, 35.41 {(×3)$(CH_3)_3$*C*C_6H_4CO-}, 13.67 (×3), 13.65 (×3), 13.42 (×3) {(×3) (*C*H_3)$_3$CC_6H_4CO-}; LC-MS $[M+1]^+$ 824.92. Analysis calcd for $C_{47}H_{53}O_{10}NO_2$: C, 68.51, H, 6.48%; found: C, 68.53, H, 6.50%.

2.3. Tested chemicals

Some partially protected derivatives of D-glucopyranoside (**Scheme 1** and **Figure 1**) were used as test chemicals. The five human bacterial pathogens and two plant fungal pathogens evaluated (**Table S1**) were from the Microbiology Laboratory, Department of Microbiology, University of Chittagong.

2.4. Antibacterial activity test

In vitro antibacterial activities of the synthesized D-glucopyranoside derivatives were carried out using the disc diffusion method.[34] Mueller Hinton agar (MHA) media was distributed in sterilized petri dishes. The bacterial suspension (0.1 ml) was placed in the sterile petri dish and about 15-20 ml of agar media was poured in. Then it was rotated clockwise and anti-clockwise, and solidification was waited for. Paper discs (5 mm in diameter) were soaked (20 µl/disc) in the tested compounds for antibacterial analysis. The diameter of the zone of inhibition was observed and measured in mm by a transparent scale. Each experiment was repeated thrice.

2.5. The Minimum inhibitory concentration (MIC) and minimum bactericidal concentration (MBC)

The MIC and MBC of the compounds showed activity against the aforementioned organisms, which was determined by applying different concentrations of the compounds alongside the same bacterial loads in a nutrient broth. MIC and MBC were determined via the broth microdilution method.[35]

2.6. Antifungal activity studies

The *in vitro* antifungal activities of the synthesized D-glucopyranoside derivatives were investigated against two plant pathogenic fungi. The “poisoned food” technique[36] was used to screen for antifungal activity, in which potato dextrose agar (PDA) was used as the culture medium. After 5 days of incubation, the diameter of the fungal radial mycelial growth was measured. The average of three measurements was taken as the radial mycelia growth of the fungus in mm.

2.7. Anticancer activity

Adult Swiss albino mice were collected from the International Center for Diarrhoeal Disease Research (ICDDR), Bangladesh. In vivo proliferation of Ehrlich’s ascites carcinoma (EAC) cells was performed according to Hasan et al.[37] The plate was agitated for 5 min and incubated at 37 °C for 1 h, and finally, the absorbance was taken at 570 nm using a titer plate reader.

2.8. Optimization and ligand preparation

Vibrational frequencies from the DMol3 code of Material Studio 08 were used to accomplish molecular optimization with DFT functional tools.[38] The functional set B3LYP and 6-31G++ were used to set the functions in DMol3 codes to obtain precise results. Once geometric optimization was done, the molecular frontier orbital diagrams were identified, HOMO and LUMO, and the optimized molecule was exported as a PDB file for molecular docking, molecular dynamics, ADMET analysis, and other in silico studies.

2.9. PAAS prediction

The pass prediction data (Pa>Pi value) was obtained from the online pass website "http://way2drug.com/PassOnline/predict.php," which is the most reliable website for predicting the bioactivity of newly synthesized molecules. Specifically, the antiviral, antifungal, anticancer, antibacterial, and antibiotic properties of the Pa> Pi value were evaluated. This value is crucial for investigating and assessing new Lead compounds' therapeutic and biological potency.[39]

2.10. Lipinski rule and pharmacokinetics

“Lipinski's rule of 5” is a guideline that is used to determine whether a compound with a specific biological or chemical activity is likely to be an orally active medication in humans. According to Christopher A. Lipinski, it was first proposed in 2001.[40] The overall value of Lipinski's rule of 5 (Hydrogen bond acceptor, Hydrogen bond donor, TPSA, Bioavailability Score, etc.) was calculated with the help of the SwissADME http://www.swissadme.ch/index.php accessible online webserver (Swiss Institute of Bioinformatics, Switzerland).[41]

2.11. Protein preparation

The crystal structure of two gram-positive and two gram-negative bacteria, including *Bacillus subtilis* (1I6W), *Escherichia coli* (1DIH), *Pseudomonas aeruginosa* (6UN1), *Staphylococcus aureus* (5YHG), and six fungal proteins such as *Aspergillus niger* (1ACZ), *Aspergillus flavus* (1XY3), *Rhizomucor miehei* (4WTP), *Mucor lusitanicus* (6ZDW), *Candida albicans* (5HW7) and *Candida Auris* (6U8J) was taken from the Protein Data Bank "https://www.rcsb.org/" where Rhizomucor miehei and Mucor lusitanicus are black Fungi, and Candida albicans and Candida Auris are white fungus protein. With a Swiss-PDBViewer (version 4.1.0) and the GROMOS96 force field, the energy reduction of all crystal structures was performed.[42] Then the PyMol (version 1.3) was employed to eliminate ligands, lipids, and heteroatoms from the crystal structure before docking.[43]

2.12. Molecular docking study and visualization

The AutoDock Vina package has been extensively used for molecular docking studies in collaboration with the PyRx Virtual Assessment Tool to accomplish docking procedures.[44] The grid centre points were set to wrap the protein's substrate-binding site, and grid box measurements were determined and set up to fit. The size of the grid boxes varied depending on the crystal structure, and Tables S2 and S3 display the dimension and centre of the grid boxes for each protein complex. Finally, a BIOVIA Discovery Studio Visualizer 2017 was sued to view the non-covalent interaction between the ligands and the pathogenic protein.[45]

2.13. Molecular dynamics simulation

With the NAMD applications, molecular dynamic simulations, have been executed in live view on a high-configuration PC.[46] Molecular dynamic simulations have substantiated the docking findings for the most potent medications up to 100 ns for holo-form (drug-protein) using the AMBER14 force field,[47] 0.9% NaCl in water was used to equilibrate the whole system at 298 degrees Kelvin temperature. During simulation, a cube was dispersed within each side of the process and periodic boundary circumstances, and was evaluated using RMSD Å and RMSF VMD.

2.14. ADMET properties

ADMET properties are one of the most significant aspects of drug molecules and are described as pharmacokinetic properties.[48] Absorption, distribution, metabolism, excretion, and toxicity (ADMET) were obtained from admetSAR, as it is one of the best websites for ADMET http://lmmd.ecust.edu.cn/admetsar2.[49] Plasma protein binding, human intestinal absorption, AMES toxicity carcinogenicity, blood-brain barrier, human oral bioavailability, and water solubility have been listed for designing ligand.

2.15. Calculation of QSAR and pIC_{50}

The quantitative structure-activity relationship (QSAR) method is one of the established methods for ligand-based drug discovery, and it was reported over 50 years ago.[50] This (QSAR) is a proven in silico approach for estimating the bioactivity of new drug molecules based on their chemical structure.[51] This open-source database gave the necessary information (including Chiv5, MRVSA9, and PEOEVSA5).[52]

3. Results and Discussion

3.1. Chemistry

D-Glucopyranoside and its derivatives are well-known carbohydrates with a glucose group exhibiting antibacterial and antifungal therapeutic efficacy.[53] This study's main aim is to know how the antimicrobial and antifungal efficacy of D-glucopyranoside compounds and their derivatives vary when the side chains are modified (**Scheme 1 and Figure 1**).

3.2. Characterization

The initial effort was to treat methyl α-D-glucopyranoside (**1**) with a 1.1 molar equivalent of 4-nitrobenzoyl chloride in DMF under freezing conditions, followed by the usual workup and separation using silica gel column chromatography, which afforded compound **2**. The FTIR spectrum (**Figure S1**) of compound **2** showed absorption bands at 1701 cm^{-1} (C=O stretching) and 3410-3510 cm^{-1} (-OH stretching), therefore suggesting the presence of carbonyl and hydroxyl groups in the molecule. In its ^{1}H-NMR spectrum (**Figure S1**), two low-field two-proton doublets at δ 8.28 (J = 8.8 Hz) and δ 8.21 (J = 8.8 Hz) corresponded to the aromatic protons of one 4-nitrobenzoyl group. The high level of deshielding of C-6 to δ 4.77 (as dd, J = 5.1 and 12.2 Hz, H-6a), 4.67 (as dd, J = 2.1 and 12.2 Hz, H-6b), as compared to its precursor {usual value (~4.00 ppm),[54,55] supported the attachment of the 4-nitrobenzoyl group at C-6. Other protons showed resonance at their usual position. The ^{13}C-NMR spectrum also showed the presence of one 4-nitrobenzoyl group by displaying the following expected resonance peaks: δ 178.12 (4-NO_2.C_6H_4.*C*O-), δ 150.86, 134.18, 130.90, 130.83, 123.64, 123.61 (4-NO_2.*C*$_6H_4$CO-). The mass spectrum of compound (**2**) had a molecular ion peak at *m/z* $[M+1]^+$ 344.29 corresponding to the molecular formula, $C_{14}H_{17}O_7NO_2$. The formation of compound (**2**) can be explained by the attachment of the 4-nitrobenzoyl group to the more reactive and less sterically hindered primary -OH group at the C-6 position, with consequent formation of methyl 6-*O*-(4-nitrobenzoyl)-α-D-glucopyranoside (**2**) as the sole product.

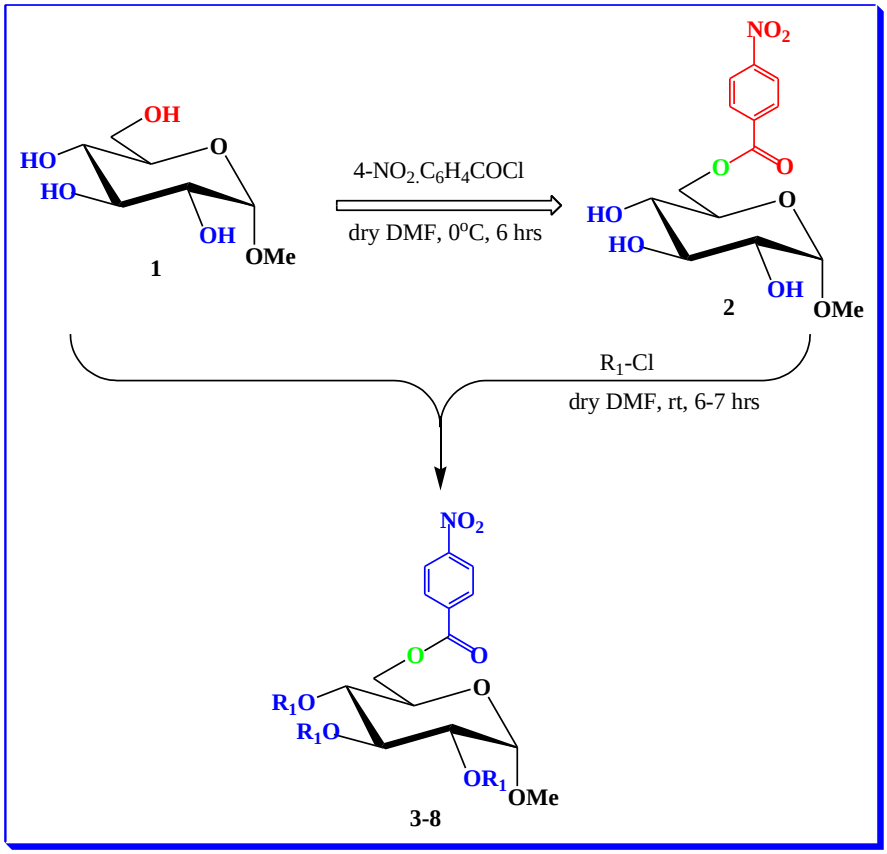

Entry	3	4	5	6	7	8
R_1	$CH_3(CH_2)_6CO$-	$CH_3(CH_2)_{14}CO$-	$CH_3(CH_2)_{16}CO$-	$(C_6H_5)_3C$-	$C_6H_5CH=CHCO$-	4-$(CH_3)_3CC_6H_4CO$-

Scheme 1. Synthesis path of the D-glucopyranoside derivatives.

The 4-nitrobenzoyl derivative **2** was then converted to the octanoyl derivative (**3**) in good yield. In its ^{1}H-NMR spectrum, two six-proton multiplets at δ 2.37 {3×$CH_3(CH_2)_5CH_2CO$-} and 1.59 {3×$CH_3(CH_2)_4CH_2CH_2CO$-}, twenty-four-proton multiplet at δ 1.28 {3×$CH_3(CH_2)_4(CH_2)_2CO$-}, and a nine-proton multiplet at δ 0.88 {3×$CH_3(CH_2)_6CO$-} due to the presence of three octanoyl groups on the molecule. The rest of the IR, ^{1}H-NMR, ^{13}C-NMR, 2D NMR, mass signals were in their anticipated positions to enable the structure of this compound as methyl 6-O-(4-nitrobenzoyl)-2,3,4-tri-O-octanoyl-α-D-glucopyranoside (**3**).

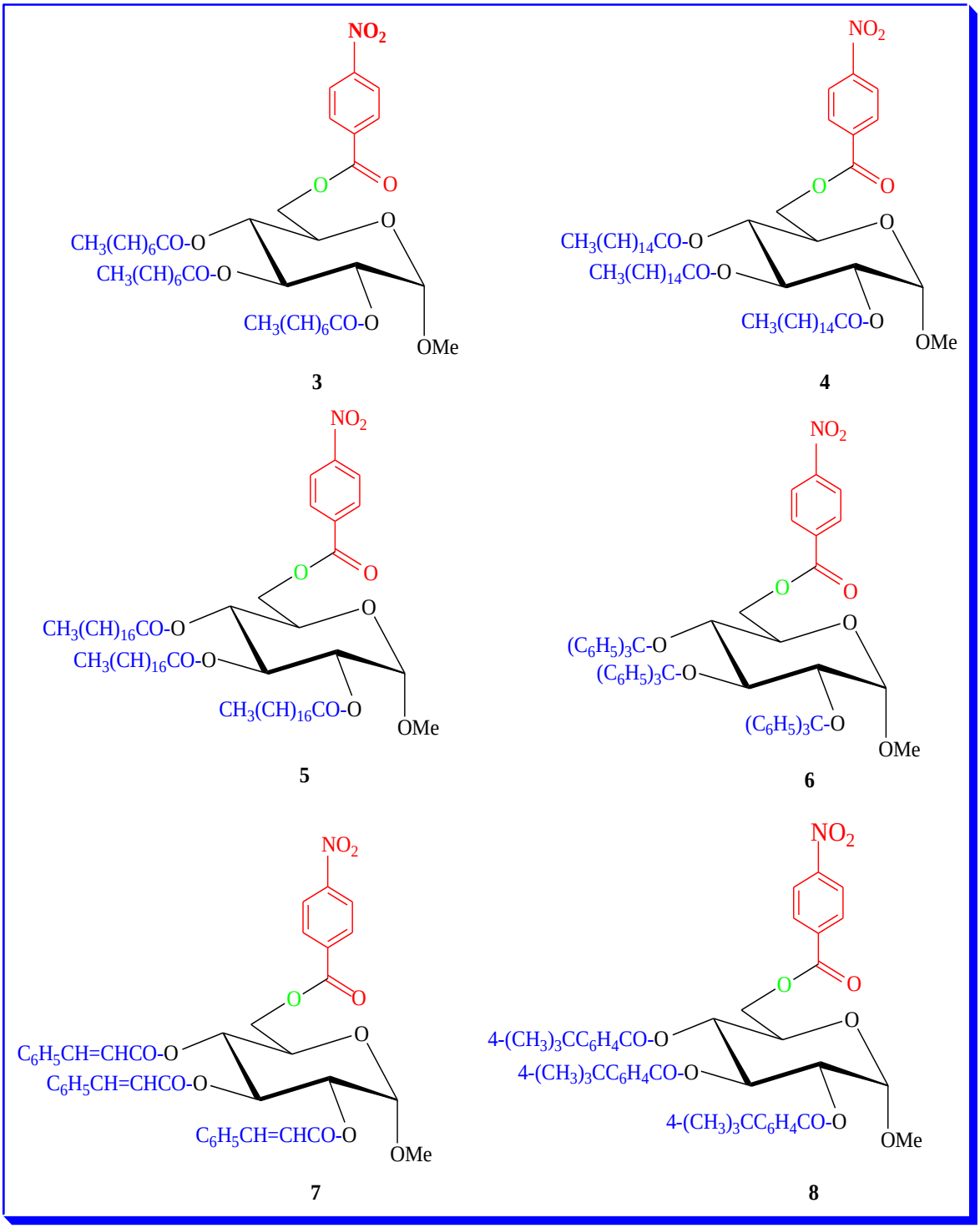

Figure 1. Chemical structures of glucopyranoside derivatives.

The 4-nitrobenzoyl product (**2**) was then derived using fatty acid chlorides, palmitoyl chloride and stearoyl chloride. Thus, the treatment of compound **2** with palmitoyl chloride and stearoyl chloride, followed by the usual work-up, produced derivatives **4** and **5** in excellent yields. On the other hand, two characteristic peaks of the ^{1}H-NMR spectrum displayed an eighteen-proton multiplet at δ 7.56 (3×Ar-H)) and a twenty seven-proton multiplet at δ 7.34 (3×Ar-H), which were due to the three trityl groups in the molecule. The rest

of the protons resonated in their anticipated positions, and this led to proposing the structure of this derivative as methyl 6-*O*-(4-nitrobenzoyl)-2,3,4-tri-*O*-trityl-α-D-glucopyranoside (**6**). Similarly, for cinnamoylation of **2** with an excess of cinnamoyl chloride in pyridine, and using the same work-up and purification techniques, the cinnamoyl derivative (**7**) was obtained. Finally, 4-*t*-butylbenzoylation of compound **2** was performed in dry DMF, furnished the 4-*t*-butylbenzoyl derivative (**8**).

3.3. Antimicrobial activity

The test compounds displayed (**Table 2**) a remarkable agonistic effect against the multitude of gram-positive and gram-negative bacterial strains above the development of the study. It was shown that derivative **8** had the highest inhibitory effect among the bacteria tested e.g., against *B. subtilis* (24±0.4 mm), and derivatives **3** and **5** displayed against *S. aureus* (22±0.3 mm) and *P. aeruginosa* (21±0.1 mm), which is higher than standard (18±0.2).[56,57] In the case of derivative **7**, the inhibitory zone is almost the same in *B. subtilis* and *P. aeruginosa* whereas when tested with derivative **6** the value of the inhibition zone was not approximately the same in *B. subtilis* and *P. aeruginosa*. Moreover, derivative **2**, showed inhibition against *B. subtilis*, *E. coli* and *S. abony*. Based on the above observation, the antibacterial activity of the derivatives can be ordered as **8**>**3**>**5**>**6**>**4** and **2** which is accordence with our previous results.[58-60]

Table 2. A zone of inhibition was observed against both the gram-positive and gram-negative bacteria. An asterisk (*) for test compounds and a double asterisk (**) for the reference antibiotic azithromycin. NI = No inhibition.

Entry	Zone of Inhibition (mm)				
	Gram-positive bacteria		Gram-negative bacteria		
	B. subtilis	***S. aureus***	***E. coli***	***S. Abony***	***P. aeruginosa***
1	NI	NI	NI	NI	NI
2	12±0.1	NI	10±0.1	13±0.1	NI
3	*19±0.1	*22±0.3	*17±0.1	*20±0.4	*18±0.3
4	13±0.2	11±0.1	NI	NI	13±0.2
5	*20±0.2	NI	*20±0.2	10±0.2	*21±0.1
6	17±0.3	NI	NI	NI	10±0.1
7	11±0.1	NI	NI	NI	13±0.3
8	*24±0.4	*20±0.3	*19±0.1	*20±0.3	*19±0.2
*Azithromycin	**18±0.2	**20±0.3	**18±0.2	**19±0.2	**19±0.2

3.4. MIC and MBC

Determination of the minimum inhibitory (MIC) and minimum bactericidal (MBC) concentrations was carried out by testing derivatives **3** and **8** against *P. aeruginosa*, *E. coli*, *S. abony*, *S. aureus* and *B. subtilis* to collect further information. As shown in **Figure 2**, the lowest MIC value was found for derivative **8** inhibiting *S. abony* (0.275±0.01mg/ml) and *S. aureus* (0.337±0.01mg/ml) in comparison with the standard Azithromycin (0.25±0.01mg/ml). The highest MIC value was recorded for derivative **3** against *E. coli* (1.55±0.01mg/ml).

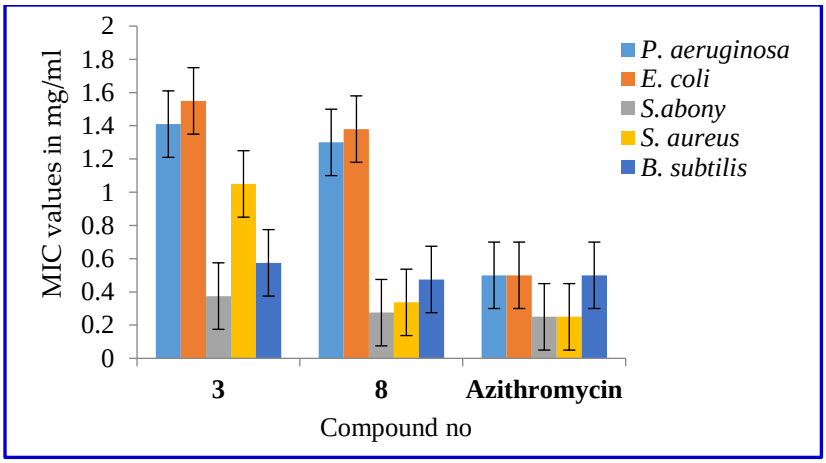

Figure 2. MIC values of the **3** and **8** compounds against tested organisms.

The lowest MBC value (1.70±0.01 mg/ml) was recorded for derivative **3** when tested against *S. aureus* in comparison with the standard Azithromycin (1.50±0.01mg/ml). The highest MBC value recorded was 5.70±0.04 mg/ml. Both derivatives **3** and **8** showed the same MBC value (2.70±0.01 mg/ml) against *B. subtilis*. The nearest MBC value (2.40±0.02 mg/ml) was also observed when compound **3** was tested against *S. abony*, and derivative **8** also displayed the same MBC against *P. aeruginosa*. MBCs are presented graphically in **Figure 3**.

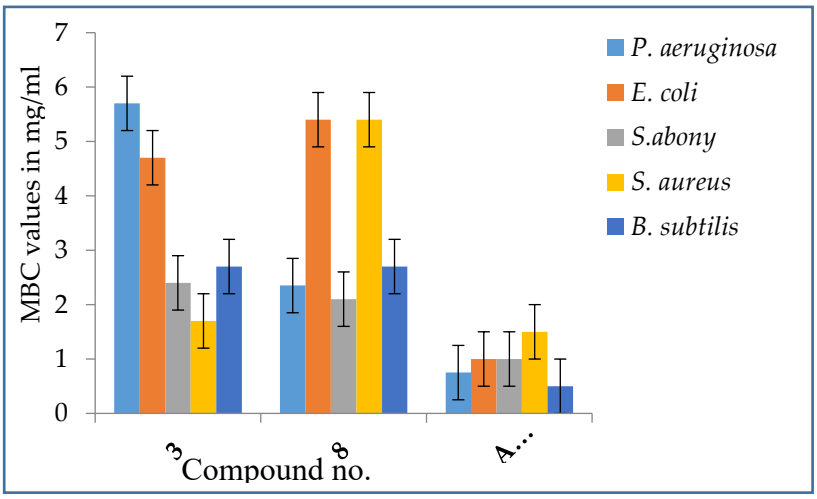

Figure 3. MBC values of the 3 and 8 compounds against tested organisms.

3.5. Antifungal activity

Antifungal activity was observed (**Table 3**) that compounds **3** and **8** opposed the growth of *A. niger* (zone of inhibition 68±1.1 mm) and *A. flavus* (zone of inhibition 72±1.0 mm), respectively. The latter value is even higher than that of the standard antibiotic, nystatin. Remarkable mycelial growth prevention was also built up for compound **6** against the *A. niger* (64 ±1.0%) and *A. flavus* (55±0.5%) in their mycelial growth test. Moreover, promising mycelial growth prevention also built up for compound **5** against the *A. niger* (63±1.0%) and *A. flavus* (57±0.5%) in the mycelial growth test. It was observed that analog **2** did not inhibit *A. niger*. Similarly, compound **4** did not inhibit *A.flavus* and the zone of inhibition was not comparable to the antibiotic Nystatin. It can be concluded that the acylation of glucopyranoside improves antimicrobial activity. The observed results reveal that the presence of different acyl moieties, including 4-*t*-butylbenzoyl, cinnamoyl, palmitoyl, stearoyl and trityl groups, significantly enhanced the antimicrobial activity of monosaccharide derivatives.[61-63]

Table 3. Antifungal activities of the synthesized test compounds in (%) of inhibition.

Entry	% Inhibition of fungal mycelial growth in mm	
	Aspergillus niger	***Aspergillus flavus***
1	NI	NI
2	NI	45±0.5
3	*68±1.1	*60±1.0
4	58±0.5	NI
5	*63±1.0	57±0.5
6	*64±1.0	55±0.5
7	52±1.0	45±0.5
8	*65±1.0	*72±1.0
** Nystatin	**66±1.0	**63±1.0

3.6. Anticancer activity

MTT assay was used to investigate the effect of *in vitro* anticancer activity on EAC cells after the screening of compounds **1-8**. The EAC cell death was found to happen in a dose-dependent manner (as shown in **Figure 4**). At 500, 250, 125, 62.5 and 31.25 µg/ml, the inhibitory effect of compound (**8**) was 25.97%, 13.82%, 6.33%, 5.83% and 4.14% respectively. When the concentration decreased gradually, the inhibitory effect also reduced and finally reached 2.03% at 15.625 µg/ml of compound (**8**).

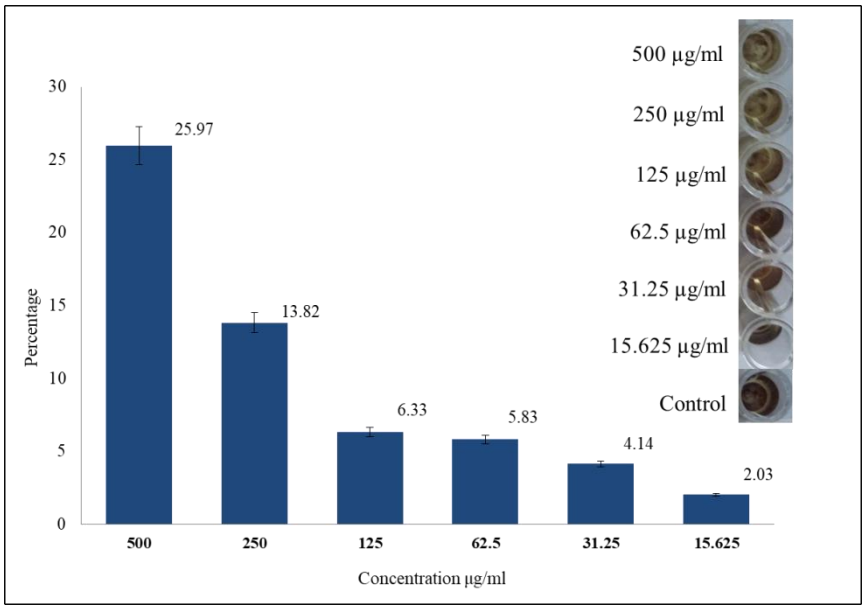

Figure 4. Anticancer activity of compound **8**.

3.7. Optimized structure of tested ligand

A DFT framework has been used to visualize the geometrical optimization of the structures of eight bioactive D-glucopyranoside and their modifications. The optimized chemical structures of these derivatives are highlighted in **(Figure S2**).

3.8. Lipinski rule, pharmacokinetics and drug ikeness

From eight potential compounds, only two reported compounds (compounds **1** and **2**) followed all the criteria and the Lipinski rule. As a result, the molecular weight of these molecules was ignored during a further computational investigation. TPSA, Å² values were found in the range of 99.38 to 169.48 whereas the molecular weights were between 194.18 and 1142.67. Secondly, the bioavailability score was 0.55 for **1**, **2**, **3**, and **7** and 0.17 for **4**, **5**, **6**, and **8**. All the designing ligands have lower G.I. absorption rates, which means they do not dissolve in the G.I. tract. In **Table S4**, the data for the Lipinski rule has been listed.

3.9. PASS prediction

Pharmaceutical research and innovation operations are designed to identify novel medicines for managing specific ailments.[64] Developing a novel drug for the market takes an average of 12 years and $800 million, with a high probability of failure (1 out of 10,000).[65] The antimicrobial spectrum was also predicted by applying the web server PASS to all compounds **1–8.** The PASS results are expressed as Pa and Pi and are displayed in **Table 4**. It can be seen in Table 3 that compounds **1–8** showed 0.43 < Pa < 0.56 for antibacterial, 0.54 < Pa < 0.66 for antifungal, 0.17 < Pa < 0.32 for antiviral and 0.26 < Pa < 0.50 for anti-carcinogenic. The attachment of additional aliphatic acyl chains increased the antifungal activity (Pa = 0.666) of the compound (1, Pa = 0.628), whereas the insertion of -$C(CH_3)_3$ substituted aromatic groups decreased the activity somewhat. Compounds **3**, **4**, and **5** showed the highest Pa value (Pa>0.666) against the fungi, whereas the highest Pa > value for antibacterial activity was observed in compound **7**. For antiviral, the highest Pa value was reported to be 0.403 in compound **1**.

Table 4. Data of PASS prediction.

	Biological Activity									
Entry	**Antiviral**		**Antibacterial**		**Antifungal**		**Antibiotic**		**Anticarcinogenic**	
	Pa	Pi	Pa	Pi	Pa	Pi	Pa	Pi	Pa	Pi
1	0.403	0.014	0.541	0.013	0.628	0.016	0.349	0.010	0.731	0.008
2	0.237	0.068	0.538	0.013	0.630	0.015	0.305	0.014	0.502	0.019
3	0.200	0.096	0.558	0.012	0.666	0.012	0.299	0.014	0.382	0.034
4	0.200	0.096	0.558	0.012	0.666	0.012	0.299	0.014	0.383	0.034
5	0.200	0.096	0.558	0.012	0.666	0.012	0.299	0.014	0.383	0.034
6	0.323	0.076	0.434	0.024	0.543	0.024	0.228	0.023	0.264	0.075
7	0.171	0.133	0.566	0.011	0.627	0.016	0.301	0.014	0.415	0.028
8	0.203	0.093	0.465	0.020	0.587	0.020	0.227	0.023	0.263	0.076
Azithromycin	0.723	0.001	0.964	0.000	0.723	0.009	0.941	0.000	N/A	N/A
Nystatin	0.210	0.087	0.967	0.000	0.986	0.000	0.946	0.000	0.416	0.028

3.10. Molecular orbitals and chemical reactivity descriptors

Any organic compounds and pharmacologically active molecules typically have a significant implication in chemical descriptors.[66] **Table S5** displays the HOMO and LUMO efficiencies for all the synthesis compounds. It has been demonstrated that as the number of functional groups and side chains (**1–8**) expanded, the hardness of these compounds steadily declined, while overall softness increased significantly. The highest electrophilicity index (ω) values for **5** (10.103 eV) and **8** (7.755 eV) indicated them to be more substantial compared to **1**, **2**, **3**, **4**, **6**, and **7**. Besides, according to the maximal hardness and minimum softness concept, these molecules **1-4** should be more reactive, more biologically active, and more acceptable to use as medications against the mentioned pathogens than compounds **5-8**.

3.11. Frontier molecular orbitals (HOMO and LUMO)

Molecular orbitals, one of the most fundamental factors towards the understanding of

chemical reactivity and kinetic predictability, are known as frontier molecular orbitals.[67] The application of the DFT approach determined HOMO and LUMO orbital configurations and the illustration is displayed in **Figure S3**. The expression, LUMO, implies the absence of electrons in circumstances where an electronegative molecule or a nucleophilic group may be readily substituted.[68] The frontier molecular orbitals are the most important in a molecule, and they are considered to study chemical reactivity and kinetic stability. It can be noted that almost all the compounds share a similar plane structure geometry, except compound **7**. This fact is related to the presence of a double bond between the phenyl ring and the carbonyl moiety. From the LUMO map analysis, we can see how this lack of double bonds affects its electronic distribution. The rest of the monosaccharide derivatives had their LUMO map with similar characteristics; the LUMO map indicated the regions of a molecule that are most sensitive to nucleophilic attack (blue color regions). One region is on the carbonyl carbon, and the other region is on the β carbon; like in a simple aromatic carbonyl compound. This fact may explain why compound **8** has anticancer activity.

3.12. Molecular of electrostatic potential (MEP) charge distribution mapping

MEP assists in the understanding of biological sensing and hydrogen bonding interrelations. With the ability to concurrently show a molecule size/shape/positive/negative/neutral electrostatic potential zone and color grading, MEP has a tremendous role to play in analyzing molecular structure/physical property correlations.[69] The electrostatic potential is represented by various colors depending on the measured value (**Figure 5**). The red color demonstrates the most negative space, which makes it a good place for an electrophilic attack. The different values of electrostatic potential are represented by different colours, with potential increases in the order red < orange < yellow < green < blue. The red colour displays the maximum negative area, which shows favorable sites for electrophilic attack; the blue colour indicates the maximum positive area favorable for the nucleophilic attack, and the green colour represents zero potential areas.

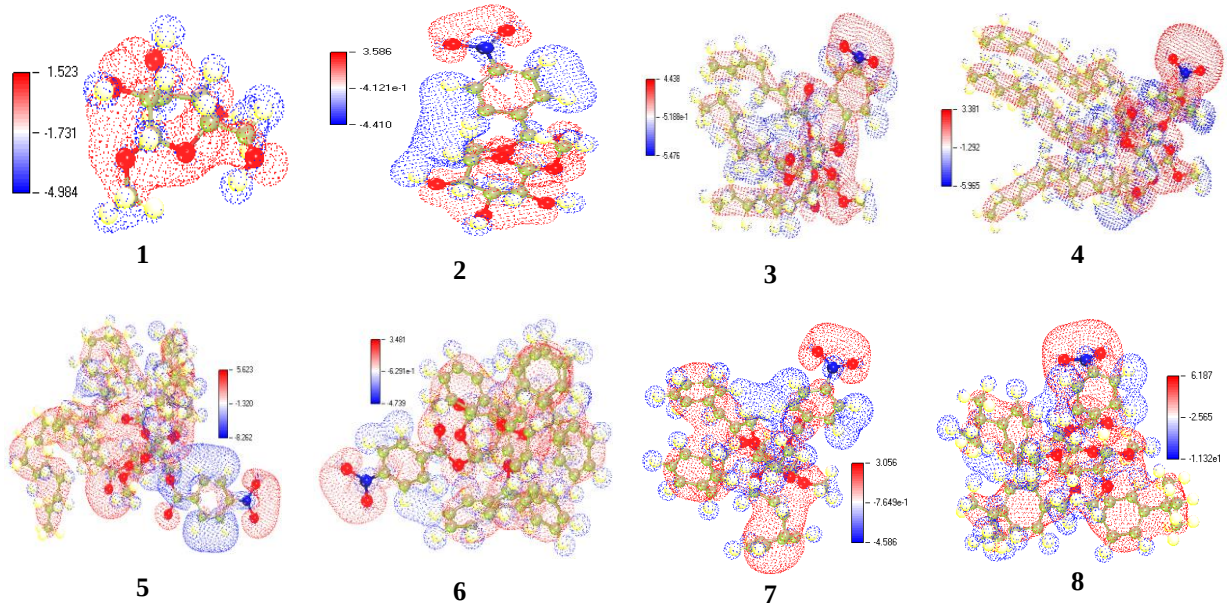

Figure 5. Molecular electrostatic potential (MEP) mappings.

3.13. Molecular docking

This method is crucial in assessing docking efficiency and showing how two molecules engage with each other. The primary causes for docking scores are hydrogen bonding and hydrophobic bonding, and the docking score of more than 6.00 kcal/mol has been regarded as a potential drug or inhibitor against particular proteases. After finishing the docking of these reported molecules, it became evident that most of the substances or ligands were more potent than the standard drug, Azithromycin, in particular, **6**, **7**, and **8** were the most potent compounds against gram-negative bacteria. Large binding affinity values were obtained for gram-positive bacteria (-9.7 kcal/mol) against B. subtilis in **6**, -9.1 kcal/mol and -

9.7 kcal/mol in **6** and **7** against *S. aureus*. For gram-negative bacteria, the most prominent binding affinity was found at -9.4 kcal/mol for **8** against *E. coli* and -9.3 kcal/mol for **6** against *P. aeruginosa*. Secondly, two more pathogenic fungi proteins such as *A. niger* and *A. flavus* were taken, and molecular docking was performed against them. It was observed that compound **6** showed at -7.9 kcal/mol against *A. niger* and -9.8 kcal/mol against *A. flavus* in compound **6**. In both gram-positive and gram-negative bacteria and fungi, the binding energy was much better than the standard compounds (**Tables S6, S7,** and **S8**).

3.14. Molecular docking against black fungus and white fungi proteins

As shown in **Tables S7** and **S8**, the most desirable results from medication development seem to have a greater affinity against white fungi and black fungi. For black fungus, the ligand-protein binding energy values obtained were at -10.4 kcal/mol and -10.0 kcal/mol in compounds **6** and **8**, respectively, against *R. miehei*. On the other hand, a value of -9.0 kcal/mol has been observed in compound **6** against *Mucor lusitanicus*, while the standard values were at -10.7 kcal/mol against *R. miehei* and -8.4 kcal/mol against *M. lusitanicus*. Secondly, for white fungus, L. **6** showed potential activity (9.3 kcal/mol and -10.5 kcal/mol) against *C. albicans* and *C. auris*, which are higher than the values for the standard compound (Nystatin). Using the Discovery Studio, researchers can determine how many bioactive peptides are present in a protein, and how they are connected to a drug or agonist. There are two primary types of bonds present in most cases (hydrogen and hydrophobic), and the electrostatic bond is also seen in some cases. Hydrophobic couplings formed for non-polar endpoints, while hydrogen-bonding couplings appeared for polar bonds. **Figures. 6, 7,** and **8** depict different binding positions for the pathogenic bacteria and fungi.

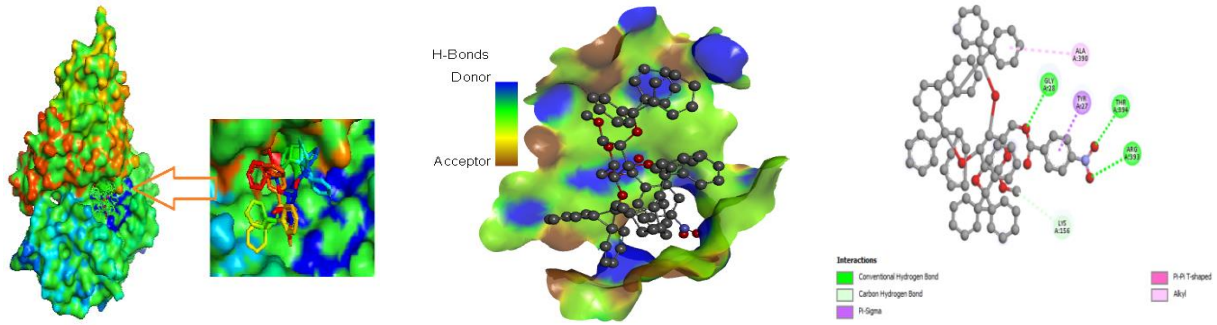

Figure 6. Molecular docking poses of *P. aeruginosa*.

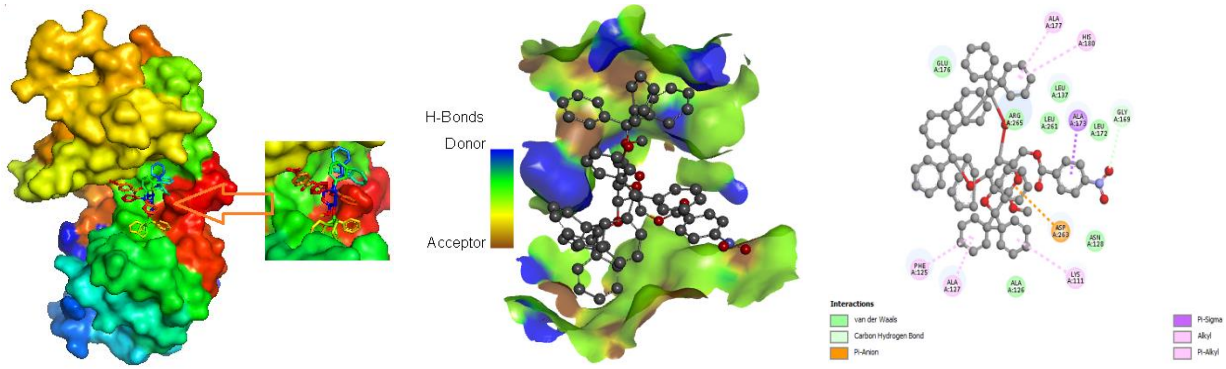

Figure 7. Molecular docking poses of *E. coli* (1DIH).

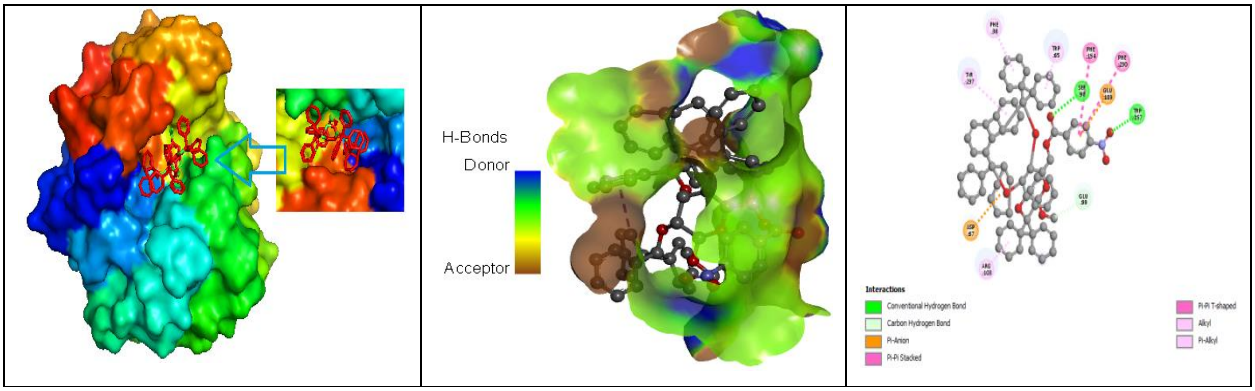

Figure 8. Molecular docking poses of *R. miehei* (4WTP).

3.15. Molecular dynamics study

It must be mentioned once again that the two terms, such as root-mean-square deviation (RMSD) and root-mean-square fluctuation (RMSF) of the ligand-protein complex, were accounted in checking the validity of the docking procedure in this study.[70] Ligand-protein docking complex with an RMSD of less than 2.0 Å are considered to be excellent fitting positions for the drug in the protein pocket, and software can appropriately validate the docking procedure for the ligand-protein complexe with their stability.[71] Next, the RMSF was calculated which indicated how the amino acid residues fluctuated throughout the docking procedure up to 100 ns time frame.

In the case of gram-negative bacteria, the compounds **6**, **7** and **8** convey a higher binding affinity against *P. aeruginosa*, as a result, the MD simulation was performed for these three complexes. There is a striking correlation between the displayed figures of the RMSD, as shown in (**Figure 9**), in regards to time and amino acid residue dependence on each other. When the time interval was 40 ns, the root-mean-square deviation (RMSD) was less than 0.7, but it increased to 0.8 at a 100 ns time interval for time vs. protein skeleton.

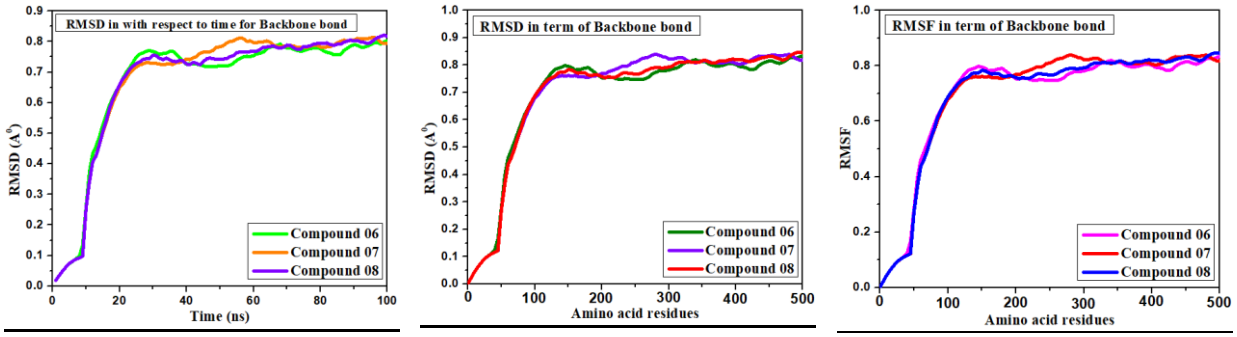

a). RMSD: Time vs protein skeleton b). RMSD: Amino acid vs backbond c) RMSF: Amino acid vs backbond

Figure 9. Various pictures of RMSD and RMSF for protein *Pseudomonas aeruginosa*.

In **Figure S4**, the RMSD value for time vs protein skeleton has been employed at 100 ns similarly accounting for the highest binding affinity after docking for compounds **6**, **7**, and **8**, the observable result is reported to be 0.9 Å, shown in 11(a), and RMSD and RMSF have unchanged amino acid vs backbone of the protein. At 250 amino acid residues, they stayed at 0.9 Å for each compound. The RMSD for protein *A. flavus* (1XY3) has been worked out at 0-100 ns (**Figure 10**).

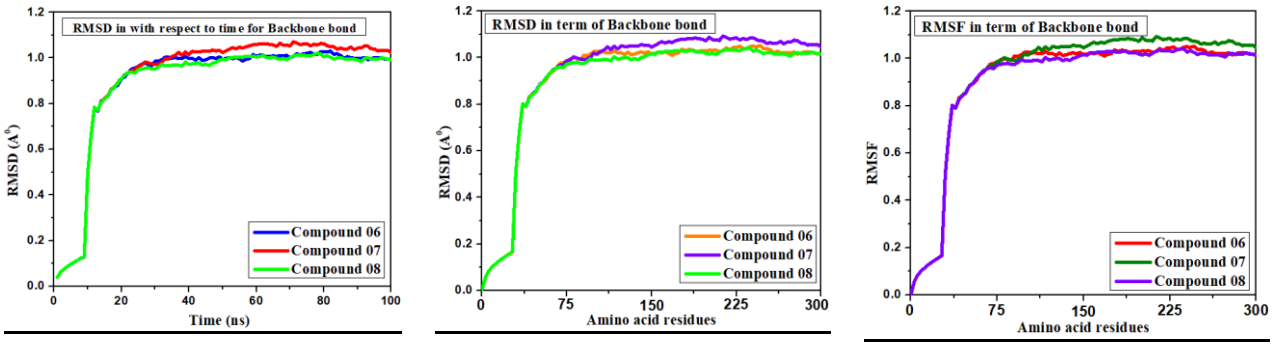

a). RMSD: Time vs protein skeleton b). RMSD: Amino acid vs backbond c) RMSF: Amino acid vs backbond

Figure 10. Various pictures of RMSD and RMSF for protein *A. flavus*.

In the illustration below in **Figure S5**, the RMSD and RMSF for protein *R. miehei* (4WTP) are recorded. The RMSD Time vs protein skeleton showed different values for each compound. At 20 ns, each compound had a similar RMSD of 0.6 Å. But, when the time interval was changed up to 100ns, 0.8 Å, 0.6 Å and 0.7 Å of RMSD were reported for compounds **6**, **7** and **8**, respectively. Similarly, the RMSD and RMSF of amino acid vs backbond were constant (0.6 Å) at 55, and different values were observed for each compound at 275 amino acid residues. The last illustration of RMSD and RMSF (**Figure S6**) displays protein *C. auris* (6U8J). Finally, it may be concluded that amino acid vs backbond is a small response for the docked complex's molecular docking affinity and stability, showing RMSD and stability. In each case, the docked complexes showed a value of less than 1.0 Å, and the docked complex vs *C. auris* (6U8J) showed 1.25 Å. Therefore, the final decision is that all the compounds were highly stable and bound perfectly with the receptor pocket. So that, the docking procedure is validated and the stability of the docked complex is maximum.

3.16. ADMET properties

ADMET investigations of compounds (**1-8**) were carried out using in-silico techniques (AdmetSAR), which predicted absorptions, distributions, metabolisms, and excretions of the compounds.[72] The compounds (**3-7**) have a positive BBB+, indicating that they can penetrate the blood-brain barrier. All of the synthesized compounds are found at a subcellular location in mitochondria. On the other hand, compounds **1**, **2** and **8** consisted of BBB- indicating that they cannot penetrate the blood-brain barrier. High Caco-2 permeability is translated into predicted log Papp values > 0.90 cm/s. As **Table 5** shows, the value of the Caco-2 permeability (log Papp) of the compounds ranged from 0.5100 to 0.5955 cm/s, log Papp<0.9 cm/s, so it is predicted that these have low Caco-2 permeability. The newly synthesized compounds possess excellent water solubility, indicating that the chemical has a greater affinity with the aqueous phase. The values for water solubility are given in log (mol/l) (insoluble ≤ -10 < poorly soluble < -6 < moderately < -4 < soluble < -2 < very soluble < 0 ≤ highly soluble). From the results shown in **Table 5**, it can be observed that the compounds tested are soluble. The water-dissolving propensity of compounds (**3-5**) was high (-4.301) compared to standard azithromycin and nystatin, and compound **1** possesses the weakest dissolving propensity (0.6210) (**Table 5**).

Table 5. ADME properties.

Entry	Human Intestinal Absorption	Caco-2 Permeability	Blood Brain Barrier	Human oral bioavailability (+ve/−ve)	P-I glycoprotein	P-II glycoprotein	Renal Organic	Sub-cellular localization	CYP450 2C9 Substrate	CYP450 1A2 Inhibitor
1	HIA-	0.8160	BBB-	HOB −	No	No	No	Mitochondria	No	No
2	HIA-	0.5955	BBB-	HOB+	Yes	No	No	Mitochondria	No	No
3	HIA+	0.5230	BBB+	HOB-	Yes	No	No	Mitochondria	No	No
4	HIA+	0.5230	BBB+	HOB-	Yes	No	No	Mitochondria	No	No
5	HIA+	0.5230	BBB+	HOB +	Yes	No	No	Mitochondria	No	No
6	HIA+	0.5100	BBB+	HOB -	Yes	No	No	Mitochondria	No	Yes
7	HIA +	0.5127	BBB +	HOB -	Yes	No	No	Mitochondria	No	Yes
8	HIA+	0.5150	BBB-	HOB -	Yes	No	No	Mitochondria	No	No
Azithromycin	HIA-	0.7578	BBB-	HOB -	Yes	Yes	No	Lysosome	No	No
Nystatin	HIA-	0.7539	BBB-	HOB -	No	Yes	No	Mitochondria	No	No

3.17. Aquatic and non-aquatic toxicity

Active pharmaceutical ingredients (APIs) have a promising possibility for interfering with the environment. They (APIs) may penetrate through patient excretions into aquatic and non-aquatic environments, and during the production processes and testing in research laboratories.[73-75] All the compounds were free from any carcinogens. The plasma protein binding score ranged from 0.159 to 1.251. An alarming result for the aquatic environment is that many of these acylated compounds responded positively to AMES toxicity (**Table S9**). Therefore, possible environmental issues with these compounds should be carefully handled.

3.18. Calculation of QSAR and pIC_{50}

This research shows that the total value of the QSAR (quantitative structure activities relationship) and pIC50 inquiry meet all of the requirements, and it has also been discovered that different compounds have varied QSAR and pIC50 values. The range of QSAR and pIC_{50} between 4.19 -9.15, whereas the higher value of QSAR and pIC_{50} is 9.15, and the lower value was found to be 4.19 (**Table 6**). The approximated pIC50 value indicates that these newly discovered compounds may become physiologically effective towards gram-positive and gram-negative bacteria, as well as against pathogenic fungi.

Table 6. Calculation of QSAR and pIC_{50}.

Comp.	Chiv5	(bcutm1)	(MRVSA9)	(MRVSA6)	(PEOEVSA5)	GATSv4	J	Diametert	pIC_{50}
1	0.752	3.733	0	0	0	0.99	2.659	6	4.19
2	1.407	3.871	11.657	39.943	0	1.234	1.796	13	4.48
3	3.893	3.882	29.565	39.943	97.821	1.327	2.265	21	5.81
4	6.893	3.89	29.565	39.943	251.921	1.384	2.103	36	8.46
5	7.643	3.892	29.565	39.943	290.446	1.354	2.061	40	9,15

6	8.485	4.059	11.657	363.001	272.987	1.182	1.11	18	6.88
7	3.732	3.897	29.885	165.857	127.452	1.339	1.231	20	6.08
8	4.468	3.938	11.657	146.12	135.11	1.332	1.322	20	6.05

4. Conclusions and Future Perspectives

For the first time, synthesized compounds have been evaluated against the aforementioned bacterial and fungal organisms. The antimicrobial screening data indicates that these tested compounds possess promising biological activities. The compounds studied showed excellent antibacterial and antifungal efficacy and are more efficient against gram-positive and gram-negative bacteria and human pathogenic fungi. Among those, compound (**8**) displayed its potential as a synthetic compound with mild anticancer activity and lower toxicity. All compounds were found to be non-carcinogenic and highly soluble in water. For pathogenic fungi, compound **6** showed -7.9 kcal/mol against A. niger and -9.8 kcal/mol against A. flavus. Considering the range of energy gap between compounds (**1-8**), compound **1** had the most significant energy gap (-9.306), and compound **5** possessed the lowest (-3.445). The lowest softness was reported as 0.215, whereas the lowest hardness was 1.836. Moreover, the molecular dynamics simulation study confirms the binding stability of the docked complex in the trajectory analysis. All methods, tools and techniques used in this work form a solid basis for the results obtained. Structural modifications of the derivatives showing the strongest activity in the present study will provide improved target compounds for the future design of antimicrobial agents.

Acknowledgments

This piece of work was supported by the Research and Publication Cell (2021-2022), University of Chittagong, Bangladesh.

Declaration of Competing Interest

The authors declare that they have no known competing financial interests or personal relationships that could have appeared to influence the work reported in this paper.

Conflicts of Interest

The authors declare no conflict of interest.

Appendix A. Supplementary data

Supplementary data to this article has been placed at the end of this article.

References

1. Bertozzi, C.R.; Kiessling, L.L. Chemical glycobiology. *Science*, **2001**, *291*, 2357–2364.
2. Chen, S.; Fukuda, M. Cell type-specific roles of carbohydrates in tumor metastasis. *Methods Enzymol.*, **2006**, *416*, 371–380.
3. Varki, A. Biological roles of oligosaccharides: all of the theories are correct. *Glycobiology*, **1993**, *3*, 97–112.
4. Shagir, A.C.; Bhuiyan, M.M.R.; Ozeki, Y.; Kawsar, S.M.A. Simple and rapid synthesis of some nucleoside derivatives: structural and spectral characterization. *Current Chem. Lett.*, **2016**, *5*, 83–92.
5. Kawsar, S.M.A.; Islam, M.; Jesmin, S.; Manchur, M.A.; Hasan, I.; Rajia, S. Evaluation of the antimicrobial activity and cytotoxic effect of some uridine derivatives. *Int. J. Biosci.*, **2018**, *12*, 211–219.
6. Amin, M.R.; Yasmin, F.; Dey, S.; Mahmud, S.; Saleh, M.A.; Emran, T.B.; Hasan, I.; Rajia, S.; Ogawa, Y.; Fujii, Y.; Yamada, M.; Ozeki, Y.; Kawsar, S.M.A. Methyl β-D-galactopyranoside esters as potential inhibitors for SARS-CoV-2 protease enzyme: synthesis, antimicrobial, PASS, molecular docking, molecular dynamics simulations and quantum computations. *Glycoconjugate J*., **2021**, *39*, 1–30.
7. Fujii, Y.; Kawsar, S.M.A.; Matsumoto, R.; Yasumitsu, H.; Naoto, I.; Dohgasaki, C.; Hosono, M.; Nitta, K.; Hamako, J.; Matsui, T.; Ozeki, Y. A-D-galactose-binding lectin purified from coronate moon turban, *Turbo (Lunella) coreensis*, with a unique amino acid sequence and the ability to recognize lacto-series glycophingolipids. *Comp. Biochem. Physiol.*, **2011**, *158B*, 30–37.
8. Devi, S.R.; Jesmin, S.; Rahman, M.; Manchur, M.A.; Fujii, Y.; Kanaly, R.A.; Ozeki, Y.; Kawsar, S.M.A. Microbial efficacy and two step synthesis of uridine derivatives with spectral characterization. *ACTA Pharm. Sci.*, **2019**, *57*, 47–68.
9. Amin, M.R.; Yasmin, F.; Hosen, M.A.; Dey, S.; Mahmud, S.; Saleh, M.A.; Hasan, I.; Fujii, Y.; Yamada, M.; Ozeki, Y.; Kawsar, S.M.A. Synthesis, antimicrobial, anticancer, PASS, molecular docking, molecular dynamic simulations and pharmacokinetic predictions of some methyl β-D-galactopyranoside analogs. *Molecules*, **2021**, *26*, 7016.
10. Scanlan, C.N.; Offer, J.; Zitzmann, N.; Dwek, R.A. Exploiting the defensive sugars of HIV-1 for drug and vaccine design. *Nature*, **2007**, *446*, 1038–1045.
11. Hart, G.W.; Housley, M.P.; Slawson, C. Cycling of *O*-linked β-N-acetylglucosamine on nucleocytoplasmic proteins. *Nature*, **2007**, *446*, 1017–1022.
12. Farhana, Y.; Amin, M.R.; Hosen, A.; Kawsar, S.M.A. Bromobenzoylation of methyl α-D-mannopyranoside: synthesis and spectral characterization. *J. Sib. Fed. Univ. Chem.* **2021**, *14*, 171–183.
13. Kawsar, S.M.A.; Hosen, M.A.; Ahmad, S.; Bakri, Y.E.; Laaroussi, H.; Hadda, T.B.; Almalki, F.A.; Ozeki, Y.; Goumri-Said S. Potential SARS-CoV-2 RdRp inhibitors of cytidine derivatives: molecular docking,molecular dynamic simulations, ADMET, and POM analyses for the

identification of pharmacophore sites. *PLoS ONE*, **2022**, *17*, e0273256.

14. Kawsar, S.M.A.; Hosen, M.A. An optimization and pharmacokinetic studies of some thymidine derivatives. An optimization and pharmacokinetic studies of some thymidine derivatives. *Turk. Comput. Theor. Chem*., **2020**, *4*, 59–66.
15. Mirajul, M.I.; Arifuzzaman, M.; Monjur, M.R.; Atiar, M.R.; Kawsar, S.M.A. Novel methyl 4,6-*O*-benzylidene-α-D-glucopyranoside derivatives: synthesis, structural characterization and evaluation of antibacterial activities. *Hacettepe J. Biol. Chem*., **2019**, *47*, 153–164.
16. Misbah, M.M.H.; Ferdous, J.; Bulbul, M.Z.H.; Chowdhury, T.S.; Dey, S.; Hasan, I.; Kawsar, S.M.A. Evaluation of MIC, MBC, MFC and anticancer activities of acylated methyl β-D-galactopyranoside esters. *Int. J. Biosci*., **2020**, *16*, 299–309.
17. Angert, E.R. Alternatives to binary fission in bacteria. *Nat. Rev. Microbiol.*, **2005**, *3*, 214–224.
18. Bulbul, M.Z.H.; Hosen, M.A.; Ferdous, J.; Chowdhury, T.S.; Misbah, M.M.H.; Kawsar, S.M.A. Thermochemical, DFT study, physicochemical, molecular docking and ADMET predictions of some modified uridine derivatives. *Int. J. New Chem.*, **2021**, *8*, 88–110.
19. Coates, A.R.; Halls, G.; Hu, Y. Novel classes of antibiotics or more of the same. *Br. J. Pharmacol.* **2014**, *163*, 184–194.
20. Prestinaci, F.; Pezzotti, P.; Pantosti, A. Antimicrobial resistance: a global multifaceted phenomenon. *Pathog. Glob. Health*., **2015**, *109*, 309–318.
21. Beigelman, P.M.; Rantz, L.A. The clinical importance of coagulase-positive, penicillin-resistant *Staphylococcus aureus*. *New Engl. J. Med*., **1950**, *242*, 353–358.
22. Thompson, C.; Young, H.; Moyes , A. Ciprofloxacin resistant Neisseria gonorrhoeae. *Genet. Med.*, **1995**, *71*, 412.
23. Starnino, S.; Stefanelli, P. Azithromycin-resistant Neisseria gonorrhoeae strains recently isolated in Italy. *J. Antimicrob. Chemother.*, **2009**, *63*, 1200–1204.
24. Rodrigues, M.L.; Nosanchuk, J.D. Fungal diseases as neglected pathogens: A wake-up call to public health officials. *PLoS Negl. Trop. Dis.*, **2020**, *14*, e0007964.
25. El-Kholy, N.A.; El-Fattah, A.M.A.; Khafagy, Y.W. Invasive fungal sinusitis in post COVID-19 patients: a new clinical entity. *Laryngoscope*, **2021**, *131*, 2652–2658.
26. Marchaim, D.; Lemanek, L.; Bheemreddy, S.; Kaye, K.S.; Sobel, J. Fluconazole-resistant Candida albicans vulvovaginitis. *Obstet. Gynocol*., **2012**, *120*, 1407–1414.
27. Sarma, S.; Kumar, N.; Sharma, S.; Govil, D.; Ali, T.; Mehta, Y.; Rattan, A. Candidemia caused by amphotericin B and fluconazole resistant Candida auris. *Indian J. Med. Microbiol.*, **2013**, *31*, 90–101.
28. Yeap, Y.Y.; Trevaskis, N.L.; Quach, T.; Tso, P.; Charman, W.N.; Porter, C.J.H. Intestinal bile secretion promotes drug absorption from lipid colloidal phases via induction of supersaturation. *Mol. Pharm.*, **2013**, *10*, 1874–1889.
29. Farhana, Y.; Amin, M.R.; Hosen, M.A.; Bulbul, M.Z.H.; Dey, S.; Kawsarm S.M.A. Monosaccharide derivatives: synthesis, antimicrobial, PASS, antiviral, and molecular docking studies against SARS-CoV-2 M^{pro} inhibitors. *J. Cellul. Chem. Technol.*, **2021**, *55*, 477–499.
30. Kawsar, S.M.A.; Hosen, M.A.; Fujii, Y.; Ozeki, Y. Thermochemical, DFT, molecular docking and pharmacokinetic studies of methyl β-D-galactopyranoside esters. *J. Comput. Chem. Mol. Model*, **2020**, *4*, 452–462.
31. Kawsar, S.M.A.; Hosen, M.A.; Alam, A.; Islam, M.; Ferdous, J.; Fujii, Y.; Ozeki, Y. Thymidine derivatives as inhibitors against novel Coronavirus (SARS-CoV-2) main protease: theoretical and computational investigations. *Adv. Chem. Res.*, **2021**, *69*, 89–129.
32. Kawsar, S.M.A.; Kumar, A. Computational investigation of methyl α-D-glucopyranoside derivatives as inhibitor against bacteria, fungi and COVID-19 (SARS-2). *J. Chil. Chem. Soci.*, **2021**, *66*, 5206–5214.
33. Kawsar, S.M.A.; Kumer, A.; Munia, N.S.; Hosen, M.A.; Chakma, U.; Akash, S. Chemical descriptors, PASS, molecular docking, molecular dynamics and ADMET predictions of glucopyranoside derivatives as inhibitors to bacteria and fungi growth. *Org. Commun.*, **2022**, *15*, 1–20.
34. Bauer, A.W.; Kirby, W.M.M.; Sherris, J.C.; Turck, M. Antibiotic susceptibility testing by a standardized single disk method. *Am. J. Clin. Pathol.*, **1966**, *45*, 493–496.
35. Melvin, P.W. Clinical and Laboratory Standards Institute (CLSI), *Performance standards for antimicrobial disk susceptibility tests*, 23rd Informational Supplement M100-S23, Clinical and Laboratory Standards Institute (CLSI), Wayne, Pa, USA, **2013**.
36. Grover, R.K.; Moore, J.D. In-vitro efficacy of certain essential oils and plant extracts against three major pathogens of Jatropha curcas L. *Phytopathology*, **1962**, *52*, 876–879.
37. Hasan, I.; Asaduzzaman, A.K.M.; Swarna, R.R.; Fujii, Y.; Ozeki, Y.; Uddin, M.B.; Kabir, S.R. MytiLec-1 shows glycan-dependent toxicity against brine shrimp Artemia and induces apoptotic death of ehrlich Ascites Carcinoma cells in vivo. *Marine Drugs*, **2019**, *17*, 1–14.
38. Lee, C.; Yang, W.; Parr, R.G. Development of the colle-Salvetti correlation-energy formula into a functional of the electron density. *Phys. Rev. B.*, **1988**, *37*, 785–789.
39. Kumaresan, S.; Senthilkumar, V.; Stephen, A.; Balakumar. B.S. GC-MS analysis and PASS-assisted prediction of biological activity spectra of extract of Phomopsis sp. Isolated from Andrographis paniculata. *World J. Pharm. Res.*, **2015**, *4*, 1035–1053.
40. Lipinski, C.A.; Lombardo, F.; Dominy, B.W.; Feeney, P.J. Experimental and computational approaches to estimate solubility and permeability in drug discovery and development. *Adv.* Drug *Deliv. Rev.*, **2001**, *46*, 3–25.
41. Daina, A.; Michielin, O.; V. Zoete. SwissADME: a free web tool to evaluate pharmacokinetics, drug-likeness and medicinal chemistry friendliness of small molecules. *Sci. Rep*., **2017**, *7*, 1–13.
42. Guex, N.; Peitsch, M.C. SWISS-MODEL and the Swiss-PdbViewer: an environment for comparative protein modeling. *Electrophoresis*, **1997**, *18*, 2714–2723.
43. Delano, W.I. The PyMOL molecular graphics system, De-Lano Scientific, San Carlos, CA, USA, **2002**.

44. Williams, C.H.; Hong, C.C. (Eds.). Chemical biology: methods and protocols. Springer, New York, USA, **2015**.

45. Version, A.D.S., 4.0. Accelrys, San Diego, USA, **2017**.

46. Abro, A.; Azam, S.S. Binding free energy based analysis of arsenic (+ 3 oxidation state) methyltransferase with *S*-adenosylmethionine. *J. Mol. Liq.*, **2016**, *220*, 375–382.

47. Case, D.A.; Cheatham 3rd, T.E.; Darden, T.; Gohlke, H.; Luo, R.; Merz Jr, K.M.; Onufriev, A.; Simmerling, C.; Wang, S.; Woods, R.J. The Amber biomolecular simulation programs. *J. Comput. Chem.*, **2005**, *26*, 1668–1688.

48. Cheng, F.; Li, W.; Zhou, Y.; Shen, J.; Wu, Z.; Liu, G.; Lee, P.W.; Tang, Y. admetSAR: A comprehensive source and free tool for assessment of chemical ADMET properties. *J. Chem. Info. Model.*, **2012**, *52*, 3099–3105.

49. Pires, D.E.V.; Blundell, T.L.; Ascher, D.B. pkCSM: predicting small-molecule pharmacokinetic and toxicity properties using graph-based signatures. *J. Med. Chem.*, **2015**, *58*, 4066–4072.

50. Hansch, C.; Fujita, T. p-σ-π Analysis. A method for the correlation of biological activity and chemical structure. *J. Am. Chem. Soc.*, **1964**, *86*, 1616–1626.

51. Judge, V.; Narasimhan, B.; Ahuja, M.; Sriram, D.; Yogeeswari, P.; Clercq, E.D.; Pannecouque, C.; Balzarini, J. Synthesis, antimycobacterial, antiviral, antimicrobial activity and QSAR studies of N2-acyl isonicotinic acid hydrazide derivatives. *Med. Chem.*, **2013**, *9*, 53–76.

52. De Oliveira, D.B.G.; Coser, A. BuildQSAR: a new computer program for QSAR analysis. *Mol. Informat.*, **2001**, *19*, 599–601.

53. Islam, S.; Hosen, M.A.; Ahmad, S.; Qamar, M.T.; Dey, S.; Hasan, I.; Fujii, Y.; Ozeki, Y.; Kawsar, S.M.A. Synthesis, antimicrobial, anticancer activities, PASS prediction, molecular docking, molecular dynamics and pharmacokinetic studies of designed methyl α-D-glucopyranoside esters. *J. Mol. Struct.*, **2022**, *1260*, 132761.

54. Hosen, M.A.; Munia, N.S.; Al-Ghorbani, M.; Baashen, M.; Almalki, F.A.; Hadda, T.B.; Ali, F.; Mahmud, S.; Saleh, M.A.; Laaroussi, H.; Kawsar, S.M.A. Synthesis, antimicrobial, molecular docking and molecular dynamics studies of lauroyl thymidine analogs against SARS-CoV-2: POM study and identification of the pharmacophore sites. *Bioorg. Chem.*, **2022**, *125*, 105850.

55. Munia, N.S.; Hosen, M.A.; Azzam, K.M.A.; Al-Ghorbani, M.; Baashen, M.; Hossain, M.K.; Ali, F.; Mahmud, S.; Shimu, M.S.S.; Almalki, F.A.; Hadda, T.B.; Laaroussi, H.; Naimi, S.; Kawsar, S.M.A. Synthesis, antimicrobial, SAR, PASS, molecular docking, molecular dynamics and pharmacokinetics studies of 5′-*O*-uridine derivatives bearing acyl moieties: POM study and identification of the pharmacophore sites. *Nucleos. Nucleot. Nucl.*, **2022**, 1–48.

56. Arifuzzaman, M.; Islam, M.M.; Rahman, M.M.; Mohammad, A.R.; Kawsar, S.M.A. An efficient approach to the synthesis of thymidine derivatives containing various acyl groups: characterization and antibacterial activities. *ACTA Pharm. Sci.*, **2018**, *56*, 7–22.

57. Ahmmed, F.; Islam, A.U.; Mukhrish, Y.E.; Bakri, Y.E.; Ahmad, S.; Ozeki, Y.; Kawsar, S.M.A. Efficient antibacterial/antifungal activities: synthesis, molecular docking, molecular dynamics, pharmacokinetic and binding free energy of galactopyranoside derivatives. *Molecules*, **2023**, *28*, 219.

58. Kabir, A.K.M.S.; Kawsar, S.M.A.; Bhuiyan, M.M.R.; Rahman, M.S.; Chowdhury, M.E.; Antimicrobial screening studies of some derivatives of methyl α-D-glucopyranoside. *Pak. J. Sci. Ind. Res.*, **2009**, *52*, 138–142.

59. Kabir, A.K.M.S.; Kawsar, S.M.A.; Bhuiyan, M.M.R.; Rahman, M.S.; Banu, B. Biological evaluation of some octanoyl derivatives of methyl 4,6-*O*-cyclohexylidene-α-D-glucopyranoside. *Chittagong Univ. J. Biol. Sci.*, **2008**, *3*, 53–64.

60. Kawsar, S.M.A., Matsumoto, R.; Fujii, Y.; Matsuoka, H.; Masuda, N.; Iwahara, C.; Yasumitsu, H.; Kanaly, R.A.; Sugawara, S.; Hosono, M.; Nitta, K.; Ishizaki, N.; Dogasaki, C.; Hamako, J.; Matsui, T.; Ozeki, Y. Cytotoxicity and glycan-binding profile of α-D-galactose-binding lectin from the eggs of a Japanese sea hare (*Aplysia kurodai*). *Protein J.*, **2011**, *30*, 509–519.

61. Bulbul, M.Z.H.; Chowdhury, T.S.; Misbah, M.M.H.; Ferdous, J.; Sujan, D.; Imtiaj H.; Yuki, F.; Ozeki, Y.; Kawsar, S.M.A. Synthesis of new series of pyrimidine nucleoside derivatives bearing the acyl moieties as potential antimicrobial agents. *Pharmacia*, **2021**, *68*, 23–34.

62. Kawsar, S.M.A.; Matsumoto, R.; Fujii, Y.; Yasumitsu, H.; Dogasaki, C.; Hosono, M.; Nitta, K.; Hamako, J.; Matsui, T.; Kojima, N.; Ozeki, Y. Purification and biochemical characterization of a D-galactose binding lectin from Japanese sea hare (*Aplysia kurodai*) eggs. *Biochem.*, (Moscow) **2009**, *74*, 709−716.

63. Shamsuddin, T.; Hosen, M.A.; Alam, M.S.; Emran, T.B.; Kawsar, S.M.A. Uridine derivatives: antifungal, PASS outcomes, ADME/T, drug-likeliness, molecular docking and binding energy calculations. *Med. Sci. Int. Med. J.*, **2021**,*10*, 1373–1386.

64. Hosen, M.A.; Alam, A.; Islam, M.; Fujii, Y.; Ozeki, Y.; Kawsar, S.M.A. Geometrical optimization, PASS prediction, molecular docking, and in silico ADMET studies of thymidine derivatives against FimH adhesin of *Escherichia coli*. *Bulg. Chem. Commun.*, **2021**, *53*, 327–342.

65. Alam, A.; Rana, K.M.; Hosen, M.A.; Dey, S.; Bezbaruah, B.; Kawsar, S.M.A. Modified thymidine derivatives as potential inhibitors of SARS-CoV: PASS, *in vitro* antimicrobial, physicochemical and molecular docking studies. *Phys. Chem. Res.*, **2022**, *10*, 391–409.

66. Cohen, N.; Benson, S.W. Estimation of heats of formation of organic compounds by additivity methods. *Chem. Rev.*, **1993**, *93*, 2419–2438.

67. Saravanan, S.; Balachandran, V. Quantum chemical studies, natural bond orbital analysis and thermodynamic function of 2,5-dichlorophenylisocyanate. *Spectrochim. Acta A Mol. Biomol. Spectrosc.*, **2014**, *120*, 351–364.

68. Alam, A.; Hosen, M.A.; Hosen. A.; Fujii, Y.; Ozeki. Y.; Kawsar, S.M.A. Synthesis, characterization, and molecular docking against a receptor protein FimH of *Escherichia coli* (4XO8) of thymidine derivatives. *J. Mex. Chem. Soc.*, **2021**, *65*, 256–276.

69. Amin, M.L. P-glycoprotein inhibition for optimal drug delivery. *Drug Target Insights*, **2013**, *7*, 27–34.

70. Maowa, J.; Alam, A.; Rana, K.M.; Hosen, A.; Dey, S.; Hasan, I.; Fujii, Y.; Ozeki, Y.; Kawsar, S.M.A. Synthesis, characterization, synergistic antimicrobial properties and molecular docking of sugar modified uridine derivatives. *Ovidius Univ. Ann. Chem*. **2021**, *32*, 6–21.

71. Kawsar, S.M.A.; Hosen, M.A.; Chowdhury, T.S.; Rana, K.M.; Fujii, Y.; Ozeki, Y. Thermochemical, PASS, molecular docking, drug-likeness and in silico ADMET prediction of cytidine derivatives against HIV-1 reverse transcriptase. *Rev. de Chim.*, **2021**, *72*, 159–178.

72. Rana, K.M.; Maowa, J.; Alam, A.; Dey, S.; Hosen, A.; Hasan, I.; Fujii, Y.; Ozeki, Y.; Kawsar, S.M.A. In silico DFT study, molecular docking, and ADMET predictions of cytidine analogs with antimicrobial and anticancer properties. *In Silico Pharmacol.*, **2021**, *9*, 1–24.

73. Fent, K.; Weston, A.A.; Caminada, D. Ecotoxicology of human pharmaceuticals. *Aqu. Toxicol.*, **2006**, *76*, 122–159.

74. Kawsar, S.M.A.; Ouassaf, M.; Chtita, S.; Jui, A.B.; Belaidi, S. PASS prediction, molecular docking and pharmacokinetic studies of acyl substituted bioactive galactopyranoside esters as antibacterial agents. *Maced. J. Chem. Chem. Eng.*, **2022**, *41*, 47–64.

75. Kawsar, S.M.A.; Almalki, F.A.; Hadda, T.B.; Laaroussi, H.; Khan, M.A.R.; Hosen, M.A.; Mahmud, S.; Aounti, A.; Maideen, N.M.P.; Heidarizadeh, F.; Soliman, S.S.M. Potential antifungal activity of novel carbohydrate derivatives validated by POM, molecular docking and molecular dynamic simulations analyses. *Mol. Simul.*, **2023**, *49*, 60–75.

Supplementary Material

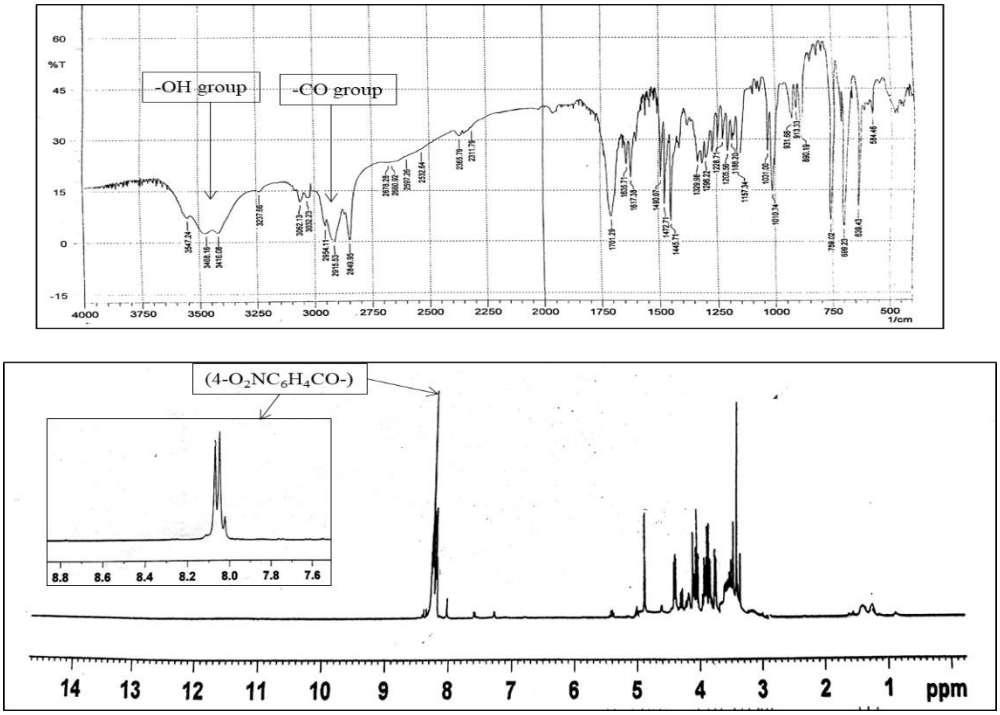

Figure S1. FTIR and ^{1}H-NMR spectra of the compound **2**.

Compound 1	Compound 2	Compound 3	Compound 4
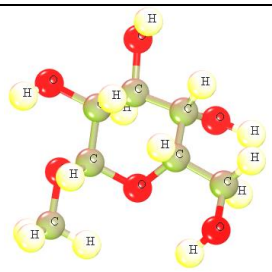	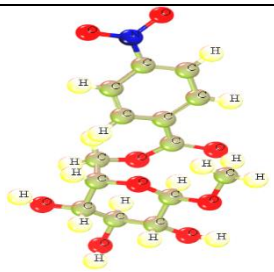	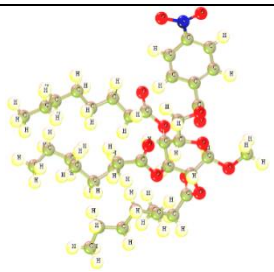	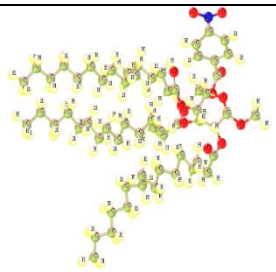
Compound 5	**Compound 6**	**Compound 7**	**Compound 8**
	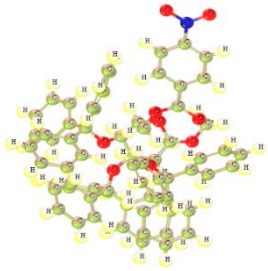	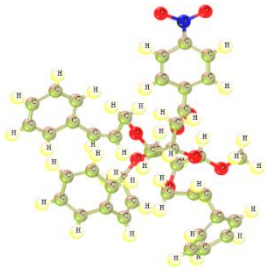	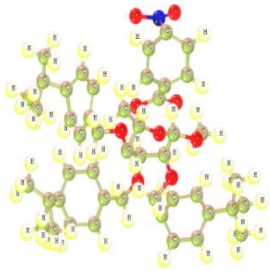

Figure S2. Optimized structure methyl α-D-glucopyranoside derivatives.

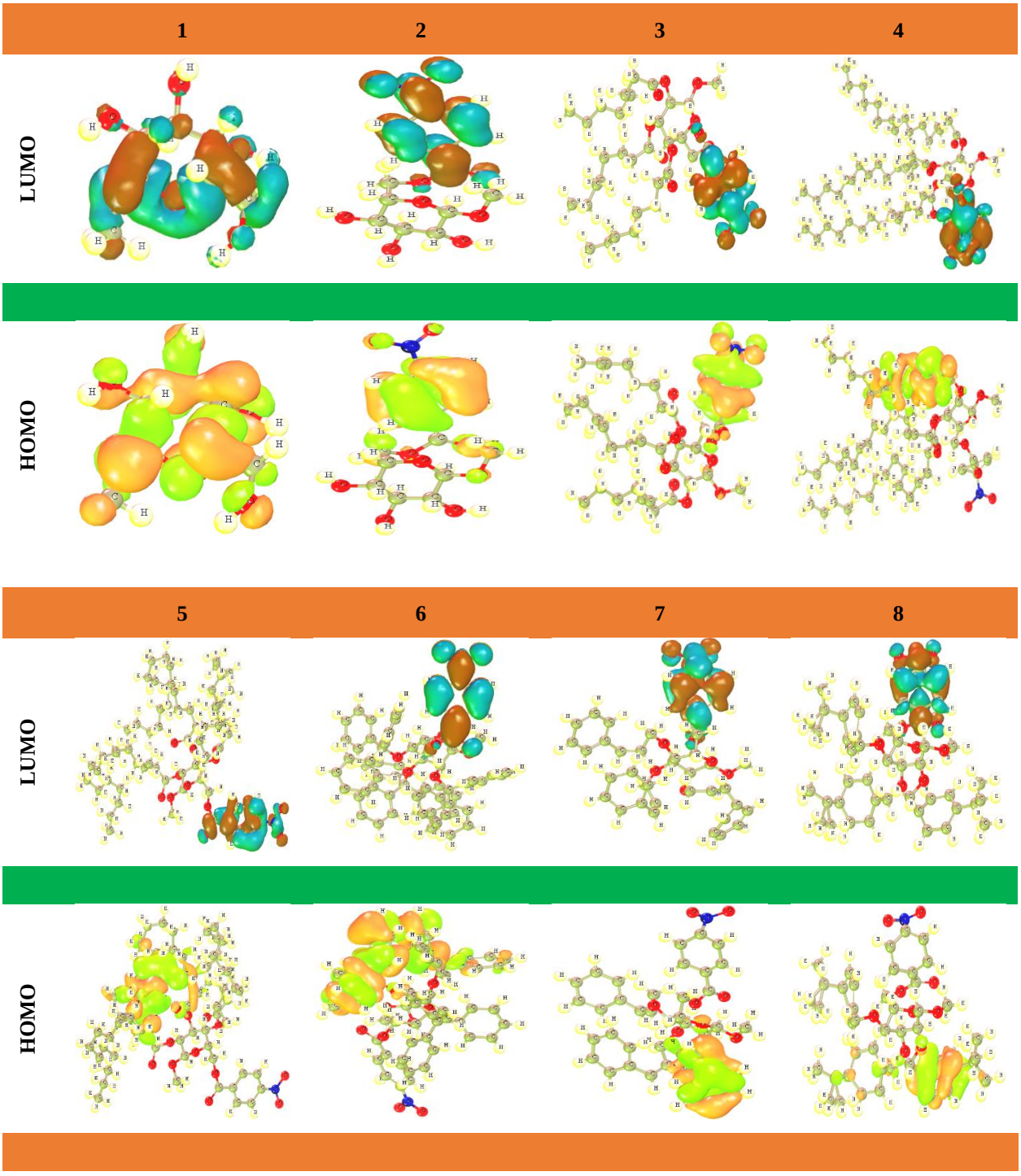

Figure S3. HOMO and LUMO diagram.

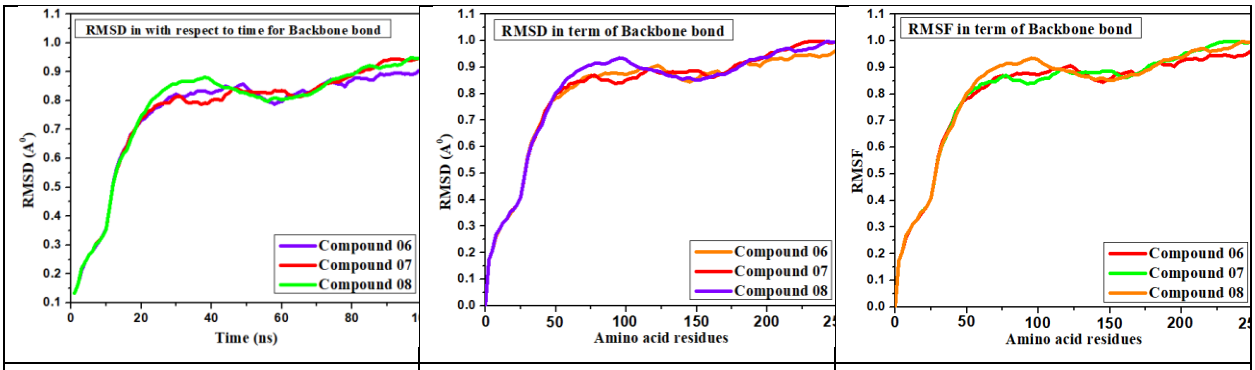

a). RMSD: Time vs protein skeleton	b). RMSD: Amino acid vs backbond	c) RMSF: Amino acid vs backbond

Figure S4. Various pictures of RMSD and RMSF for protein *E. coli*.

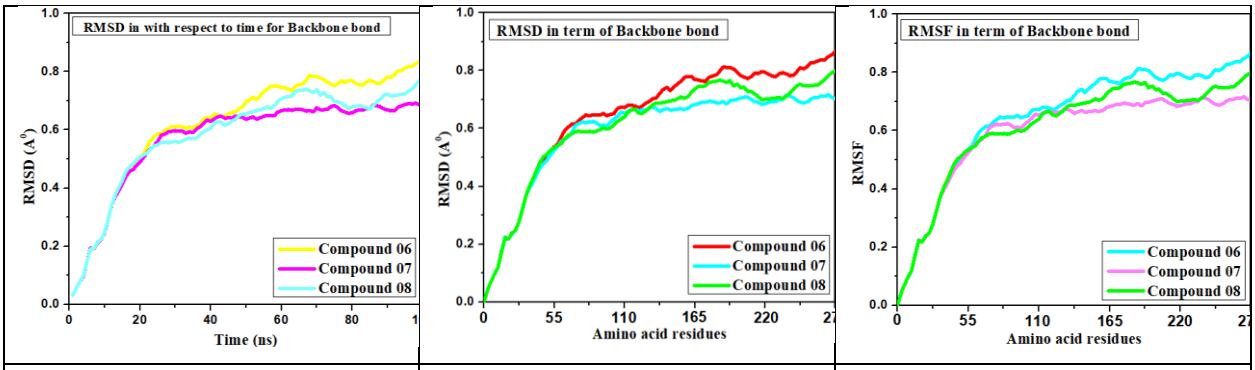

a). RMSD: Time vs protein skeleton	b). RMSD: Amino acid vs backbond	c) RMSF: Amino acid vs backbond

Figure S5. Various pictures of RMSD and RMSF for protein *R. miehei*.

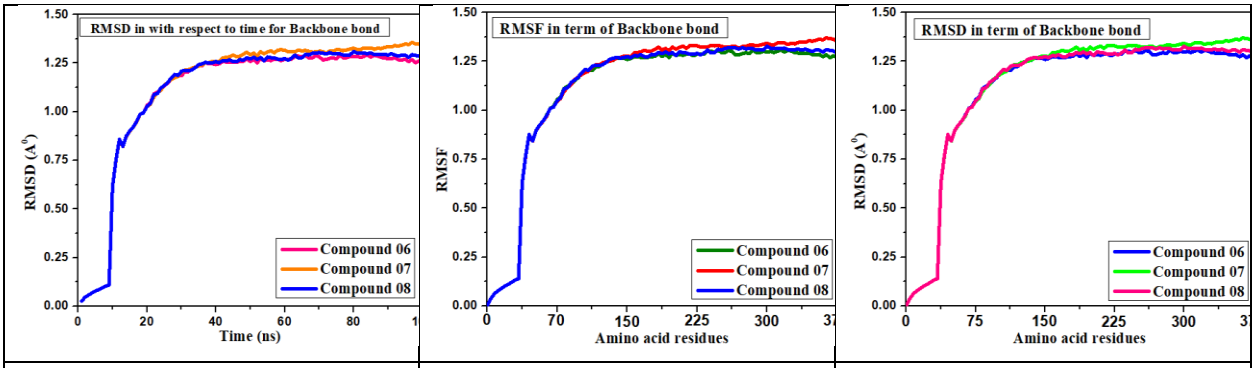

a). RMSD: Time vs protein skeleton	b). RMSD: Amino acid vs backbond	c) RMSF: Amino acid vs backbond

Figure S6. Various pictures of RMSD and RMSF for protein *C. Auris*.

Table S1. Bacterial and fungal pathogens used in this study.

Type	Microorganism	Strain no.
	Bacteria	
Gram +Ve	*Bacillus subtilis*	ATCC 6633
	Staphylococcus aureus	ATCC 6538
	Escherichia coli	ATCC 8739
Gram -Ve	*Pseudomonas aeruginosa*	ATCC 9027
	Salmonella abony	NCTC 6017
	Fungus	
	Aspergillus niger	ATCC 16404
	Aspergillus flavus	ATCC 204304

Table S2. Grid box parameters used for docking analysis in this study for bacteria.

	Grid box size	
Protein Name with the PDB ID	**Dimension (Å)**	**Center**
Aspergillus niger (1ACZ)	X: 30.8323 Y: 47.5945 Z: 30.5023	X: − 0.0130 Y: 1.1682 Z: 0.7184
Aspergillus flavus (1XY3)	X: 92.3443 Y: 125.5613 Z: 149.4790	X: − 15.4559 Y: − 18.998 Z: 97.0035
Eschercia coli (1DIH)	X: 48.0575 Y: 41.7442 Z: 51.5023	X: 14.3218 Y: 27.7359 Z: 51.5023
Pseudomonas aeruginosa (6UN1)	X:56.9842 Y:63.7870 Z:97.7176	X:6.0802 Y:19.5472 Z:2.1794

Table S3. Grid box parameters used for docking analysis in this study for fungi.

Grid box size		
Protein Name with the PDB ID	**Dimension (Å)**	**Center**
Aspergillus niger (1ACZ)	X: 30.8323 Y: 47.5945 Z: 30.5023	X: − 0.0130 Y: 1.1682 Z: 0.7184
Aspergillus flavus (1XY3)	X: 92.3443 Y: 125.5613 Z: 149.4790	X: − 15.45 Y: − 18.998 Z: 97.0035
Rhizomucor miehei (4WTP)	X: 48.0575 Y: 41.7442 Z: 51.5023	X: 14.3218 Y: 27.7359 Z: 51.5023
Mucor lusitanicus (6ZDW)	X: 57.4044 Y: 55.5974 Z: 41.1118	X: 36.6352 Y: 22.1218 Z: 55.6026
Candida albicans (5HW7)	X: 43.3127 Y: 43.5687 Z: 60.4094	X: 13.1631 Y: 93.6564 Z: 23.3036
Candida auris (6U8J)	X: 102.5392 Y: 107.3948 Z: 210.2020	X: 3.9837 Y: 70.6740 Z: 67.2068

Table S4. Data of lipinski rule, pharmacokinetics and drug likeness.

Entry	**NBR**	**HBA**	**HBD**	**TPSA, Å²**	**Consensus Log Po/w**	**Log Kp (skin permeation), cm/s**	**Lipinski rule**		**M.W.**	**Bioavailability Score**	**G.I. absorption**
							Result	**Violation**			
1	02	06	04	99.38	-1.86	-9.37	Yes	0	194.18	0.55	Low
2	06	09	03	151.27	-0.75	-8.78	Yes	0	343.39	0.55	Low
3	30	12	00	169.48	6.80	-3.49	No	2	721.87	0.55	Low
4	54	12	00	169.48	15.31	3.69	No	3	1058.51	0.17	Low
5	60	12	00	169.48	17.02	5.48	No	3	1142.67	0.17	Low
6	21	09	00	118.27	10.73	-2.11	No	2	1070.23	0.17	Low
7	18	09	00	118.27	N/A	N/A	N/A	N/A	697.87	0.55	Low
8	18	09	99	118.27	7.87	-3.57	No	2	791.97	0.17	Low
Azithromycin 447043	07	14	05	180.08	2.02	-8.01	No	2	748.98	0.17	Low
Nystatin 14960	03	18	12	319.61	-0.18	-12.09	No	3	926.1	0.17	Low

[TPSA: Topological polar surface area, Consensus Log: Logarithm of partition coefficient between n-octanol and water**,** NBR: Number of rotatable bonds**,** HBA: Hydrogen bond acceptor, HBD: Hydrogen bond donor**,** M.W: Molecular weight, G.I. Absorption: Gastrointestinal absorption].

Table S5. Data of chemical descriptors.

S/N	A=-LUMO	I=- HOMO	Energy =I-A	Chemical potential $(\mu) = -\frac{I+A}{2}$	Electronegativity $(\chi) = \frac{I+A}{2}$	Hardness $(\eta) = \frac{I-A}{2}$	Softness $(\sigma) = \frac{1}{\eta}$	Electrophilicity $(\omega) = \frac{\mu^2}{2\eta}$
1	-1.593	-10.899	-9.306	-6.246	6.246	4.653	0.215	4.192
2	-3.183	-10.500	-7.317	-6.842	6.842	3.659	0.273	6.397
3	-2.613	-9.406	-6.793	-6.010	6.010	3.397	0.294	5.316
4	-3.127	-8.076	-4.949	-5.602	5.602	2.475	0.404	6.340
5	-4.177	-7.622	-3.445	-5.900	5.900	1.713	0.581	10.103
6	-2.641	-8.060	-5.419	-5.351	5.351	2.710	0.369	5.283
7	-3.102	-7.408	-4.306	-5.255	5.255	2.153	0.464	6.413
8	-3.500	-7.171	-3.671	-5.336	5.336	1.836	0.545	7.755

Table S6. Docking score against Gram-negative bacteria.

	***E. coli* (1DIH)**				***Pseudomonas aeruginosa* (6UN1)**			
Entry	**Binding Affinity (kcal/mol)**	**No of H bond**	**No of Hydrophobic bond**	**No of Electrostatic Bond**	**Binding Affinity (kcal/mol)**	**No of H bond**	**No of Hydrophobic bond**	**No of Electrostatic Bond**
1	-5.0	01	00	00	-5.5	04	00	00
2	-7.2	08	01	01	-7.9	09	04	00
3	-6.8	10	11	00	-6.3	09	05	00
4	-5.2	01	13	00	-5.4	05	15	00
5	-4.6	06	11	01	-5.7	06	15	00
6	-8.4	01	06	01	-9.3	03	09	01
7	-7.9	05	07	00	-7.7	10	04	00
8	-9.4	05	08	01	-7.2	06	08	00
Azithromycin	-7.8	04	04	00	-6.9	03	07	00

Table S7. Docking score against fungi.

	Aspergillus Niger (1ACZ)				*Aspergillus flavus* (1XY3)			
Entry	**Binding Affinity (kcal/mol)**	**No of H bond**	**No of Hydrophobic bond**	**No of Electrostatic Bond**	**Binding Affinity (kcal/mol)**	**No of H bond**	**No of Hydrophobic bond**	**No of Electrostatic Bond**
1	-4.7	03	00	00	-5.8	08	00	00
2	-6.2	05	02	00	-7.7	06	01	00
3	-5.9	07	08	00	-6.5	04	09	01
4	-4.6	02	16	00	-5.9	03	16	00
5	-4.6	00	14	00	-6.5	07	15	00
6	-7.9	02	03	00	-9.8	01	05	01
7	-6.5	05	03	00	-7.2	03	05	01
8	-7.1	03	05	00	-8.8	04	05	02
Nystatin	-7.8	10	00	00	-10.0	9	03	00

Table S8. Docking score against white fungi.

	Candida albicans (5HW7)				*Candida Auris* (6U8J)			
Entry	**Binding Affinity (kcal/mol)**	**No of H bond**	**No of Hydrophobic bond**	**No of Electrostatic Bond**	**Binding Affinity (kcal/mol)**	**No of H bond**	**No of Hydrophobic bond**	**No of Electrostatic Bond**
1	-4.9	01	00	00	-6.0	04	00	00
2	-6.5	03	03	01	-7.0	02	03	00
3	-5.6	03	08	00	-7.3	04	05	00
4	-5.9	06	14	00	-6.4	05	13	00
5	-4.7	05	11	00	-7.0	05	20	00
6	-9.3	04	04	01	-10.5	01	04	02
7	-6.9	01	07	00	-9.0	03	11	01
8	-8.0	02	05	00	-10.0	03	08	00
Nystatin	-9.0	07	01	00	-10.0	09	00	00

Table S9. Aquatic and non-aquatic toxicity

Entry	AMES toxicity	Carcino genicity	Water solubility, Log S	Plasma protein binding	Acute Oral Toxicity, kg/mol	Oral Rat Acute Toxicity (LD50) (mol/kg)	Fish Toxicity pLC50 mg/L	T. Pyriformis toxicity (log ug/L)
1	No	No	0.621	0.159	0.4849	1.1350	2.6152	-1.1613
2	No	No	-2.633	0.82	0.6561	2.3915	1.2948	0.7979
3	Yes	No	-4.301	1.179	0.5687	2.7011	0.7794	1.3483
4	Yes	No	-4.301	1.251	0.5687	2.7011	0.7794	1.3483
5	Yes	No	-4.301	1.227	0.5687	2.7011	0.7794	1.3483
6	Yes	No	-3.365	1.076	0.6203	2.5951	0.8673	1.1276
7	Yes	No	-3.415	1.031	0.6730	2.4304	0.8356	1.0898
8	Yes	No	-3.820	0.928	0.5633	2.7576	0.7511	1.0998
Azithromycin	No	No	-2.060	0.823	0.7761	2.5423	1.5567	0.4275
Nystatin	No	No	-3.091	0.973	0.7227	2.2357	1.5706	0.4977